



Flexible N-layer composite beam/column elements with interlayer partial interaction imperfection—A novel approach to structural stability and

Downloaded from: <https://research.chalmers.se>, 2025-06-11 22:42 UTC

Citation for the original published paper (version of record):

Atashipour, R., Challamel, N., Girhammar, U. et al (2025). Flexible N-layer composite beam/column elements with interlayer partial interaction imperfection—A novel approach to structural stability and dynamic analyses. *Composite Structures*, 367. <http://dx.doi.org/10.1016/j.compstruct.2025.119219>

N.B. When citing this work, cite the original published paper.



Flexible N -layer composite beam/column elements with interlayer partial interaction imperfection—A novel approach to structural stability and dynamic analyses

Seyed Rasoul Atashipour^{a,*}, Noël Challamel^b, Ulf Arne Girhammar^c, Peter D. Folkow^a

^a Division of Dynamics, Department of Mechanics and Maritime Sciences (M2), Chalmers University of Technology, SE-412 96 Gothenburg, Sweden

^b Université de Bretagne Sud, UBS – Institut de Recherche Dupuy de Lôme IRDL (CNRS UMR 6027), Centre de Recherche, Rue de Saint Maudé, BP 92116, 56321 Lorient Cedex, France

^c Department of Engineering Sciences and Mathematics, Division of Wood Science and Engineering, Luleå University of Technology, Skellefteå, Sweden

ARTICLE INFO

Keywords:

Interlayer partial interaction imperfection
Partial-composite models
Flexible number of identical constituting layers
Buckling and vibration formulae
Conversion coefficient

ABSTRACT

Existing vibration and buckling analysis models for the partial-composite beam/column elements are restricted to a limited number of constituting layers. This is due to the escalated complexity of the governing equations with an increase in the number of layers. The present study formulates the stability and vibration problems of columns and beams composed of any number of identical constituting layers, incorporating the effects of interlayer partial-interaction imperfection. A Timoshenko/Engesser-hypothesis-based partial-composite (TEPC) model is developed and a novel analytical solution scheme is implemented into the extracted governing differential equations. As a result, efficient conversion coefficients are introduced, converting the well-known classical Euler column buckling and beam vibration formulae to those of multilayer elements having interlayer partial-interaction imperfection based on the TEPC model. The validity of the proposed approach is verified through comparison with available experimental data and the conducted 3-D FEA. It is shown that the most significant reduction in the predicted buckling capacity of partial-composite multilayer columns, when transitioning from the EBPC model to TEPC, occurs for the columns with the highest interlayer interaction. Furthermore, it is shown that the influence of interlayer interaction level on the Euler-to-Timoshenko/Engesser conversion coefficients becomes less pronounced as the number of constituting layers increases.

1. Introduction

Layered composite structural elements are omnipresent in a broad range of modern engineering applications, from marine structures and underwater vehicles [1–3], aviation and aerospace structures [4–7] to infrastructure and advanced building structures [8–10]. This widespread application is due to their superior mechanical properties and performance [11]. However, inevitable imperfections, arising from production to implementation [12], play a crucial role in the functionality and reliability of composite structures [13], resulting in degraded mechanical behavior and performance.

Imperfections in layered composite elements may be geometrical (such as initial deflection and out-of-straightness [14–17], geometrical gaps and waviness/wrinkles in the layers [12,18,19], layers thickness variation [20,21], and loading eccentricity and boundary condition

imperfections [22–24]), or of material and constructional type (e.g., cracks and partial delamination [25–27], interfacial bonding defects such as incomplete/uneven/poor bonding, or interfacial shear slip [28–35], etc.).

The influence of interfacial bonding imperfection on the mechanical behavior of layered structures has been studied extensively by many researchers, modeling imperfect bonding behavior using linear spring-like models [36–38] or based on nonlinear elastic/elastoplastic/visco-elastic models [33,39,40] in computational simulations. A commonly referred theory in structural applications for studying the effects of a specific type of interfacial imperfection, in the form of interlayer partial-composite interaction (e.g., in layered timber composites), is known as the “partial-composite” theory [41–44]. This theory captures the interlayer partial interaction in the form of relative slip via a shear spring-like model. It should be noted that the present study is primarily focused on

* Corresponding author.

E-mail address: rasoul.atashipour@chalmers.se (S.R. Atashipour).

<https://doi.org/10.1016/j.compstruct.2025.119219>

Received 29 October 2024; Received in revised form 1 March 2025; Accepted 24 April 2025

Available online 5 May 2025

0263-8223/© 2025 The Author(s). Published by Elsevier Ltd. This is an open access article under the CC BY license (<http://creativecommons.org/licenses/by/4.0/>).

this specific type of imperfection. Consequently, any other forms of interfacial bonding imperfections are beyond the scope of this article.

In laminated timber composite structures, various types of mechanical connectors, such as bolts, nails, dowels, and screws, or adhesives, are applied to keep the integrity of the structures. As a consequence, their structural behavior and performance may deviate from those of perfect ideal composites due to the relative interlayer slips. Initial efforts to formulate such an imperfect partial-interaction complex mechanical behavior may be attributed to Stüssi, Switzerland, 1947 [45], Rzhantsyn, Russia, 1948 [46], Granholm, Sweden, 1949 [47], Newmark et al., USA, 1951 [48], and Pleshkov, Russia, 1952 [49], who independently developed the governing static equations for the timber composite beams with partial interaction. For a detailed literature background on the partial-composite theory, readers are referred to [41].

The vast majority of the research studies related to the layered partial composites in the literature focus on different aspects of two-layer- and, to a lesser extent, three-layer structures. Static bending analysis of two-layer partial-composite beams was performed by Faella et al. [50] and Ranzi et al. [51], respectively, based on analytical solutions and a finite element model. Jurkiewicz et al. [52], and Ranzi and Bradford [53] developed a numerical and an analytical model for the time-dependent behavior of two-layer composite beams with partial interaction imperfection, respectively. Girhammar and Pan [41] and Girhammar [42] introduced the governing differential equations and general analytical solutions for the first- and second-order static analyses of two-layer partial-composite beams and beam-columns on the basis of the Euler-Bernoulli kinematics assumptions. Xu and Wu [54] generalized the first-order analyses by taking into account the influences of rotary inertia and shear deformations according to the Timoshenko hypothesis and the Engesser's approach for each layer with the same rotation. Schnabl and Planinc [55] investigated the buckling of two-layer Timoshenko beams, including the extensibility effect and the differential shear assumptions of Haringx's theory (i.e., the possibility of having different rotation kinematics for each layer). Santos and Silberschmidt [56] introduced an equilibrium-based finite element formulation for the static analysis of Timoshenko partial composites. Ecsedi and Baksa [57] developed an analytical model to analyze the deformation and stresses in two-layer composite beams with partial interaction imperfection based on the Timoshenko kinematics and assuming the same cross-sectional rotation in the two layers.

With regard to the vibration and dynamic analyses of two-layer composite elements having interfacial partial-interaction imperfection, readers are referred to the research by Girhammar et al. [44] for the free and forced in-plane vibrations, Challamel [58] for the lateral-torsional vibration, and Challamel et al. [59] for the out-of-plane vibration problems. He and Yang [60] implemented a higher-order beam theory for dynamic analysis of two-layer composite beams with partial interaction. Regarding research on the application of the partial-composite theory to buckling and stability problems, a series of research works by Challamel and Girhammar [61–63] can be pointed out for, e.g., the linear in-plane and lateral-torsional buckling, and the geometrically nonlinear post-buckling analyses of two-layer partially-bonded imperfect columns based on the uniform and the differential shear deformable kinematics assumptions. Similar to [61], Le Grogneq et al. [64] also investigated the in-plane buckling of two-layer partial-composite beams, considering the Engesser's differential shear model and obtained similar results. The problem of thermal buckling of two-layer shear deformable beams with interlayer partial interaction imperfection was treated by Komijani et al. [65].

Despite several research in the literature addressing different aspects of the structural mechanic behavior of two-layer partial composites, less attention has been drawn to those having a higher number of constituting layers. A key reason is that the governing equations of the partial-composite theory are dependent on the number of constituting layers and, therefore, their complexity dramatically increases when the

number of constituting layers is raised. For the research on three-layer partial-interaction composites, readers are directed to the recent research studies by Atashipour and his co-workers [66,67] for the structural buckling of shear deformable columns, and the heavy columns under varying axial compressive loads; Nguyen et al. [68] and Sun et al. [69] for the dynamic based on an analytical approach and a finite element (FE) model; and Lin et al. [70] for the static and vibration response and analyses using an FE technique. Also, Atashipour et al. [71] studied the weak shear web effects of a deep timber element in bending by modeling it as a three-layer composite beam with equivalent partial-bonding imperfection.

Due to the complexity of the governing equations of the multilayer structures with the interlayer partial interaction imperfection, the amount of published research in the literature for multilayer composites is limited, where they mostly suffer from a lack of general analytical solutions. Heinisuo [72] introduced an FE formulation for some particular three- and five-layered beam elements with some limitations on the shapes and properties of the cross-section; nevertheless, numerical instabilities were reported. Krawczyk and his co-workers [73,74] developed a layerwise geometric nonlinear FE scheme for multilayer beams with partial interaction. Ranzi [75] also presented an FE formulation on the basis of the weak form and Euler-Bernoulli kinematic assumptions for the multilayer beams with partial interaction imperfection. Sousa Jr and da Silva [76] studied the static behavior of the general case of multilayered composite beams with interlayer slip based on analytical formulations and a numerical finite element solution approach. Also, based on Timoshenko's kinematic assumptions, Keo et al. [77] presented a shear-deformable finite element formulation for multilayered beams in partial interaction. Recently, Adam et al. [78] studied moderately large vibrations of partial-composite layered beams using a semi-analytic solution for the symmetrically layered three-layer beams, and using Galerkin and Ritz numerical methods for a higher number of layers. Häggbom [79] derived the linear buckling governing differential equations of multilayer Euler columns with identical constituting layers and derived an analytical solution for the simply-supported members. Ylinen [80], reconsidered the same problem using the same methodology, and obtained an alternative analytical formula. The methodology of Häggbom [79] and Ylinen [80] is based on the reduction of the coupling system of differential equations for the N -layer beam problem in a mixed spatial differential-difference equation. Assuming a trigonometric solution of the deflection in the longitudinal direction gives a difference equation to be solved in the transversal direction. The same methodology was used by Bolotin [81] (see also Bolotin and Novichkov [82]) who also solved a difference equation for the static bending of multilayered plates with N identical layers. Recently, Peng et al. [83] analytically investigated the static bending of multilayered beams and plates under distributed load for N equivalent layers. Also, Shen et al. [84] studied the bending of multilayered beams with equivalent layers, using an equivalent approximate continuous beam model.

To the best of the authors' knowledge, no exact analytical solutions and efficient explicit formulae for the buckling and vibrations of multilayer columns/beams having interlayer partial-interaction imperfection are available in the literature without limitation with respect to the number of constituting layers. To fill this apparent void, the present work is conducted to provide exact analytical solutions for buckling and vibrations of N -layer shear-deformable partial-composite columns/beams for the first time. Accordingly, explicit buckling and vibration formulae are introduced in an efficient simple form without any approximation or limitation with respect to the number of constituting layers. An Euler-Bernoulli- (EBPC) and a Timoshenko/Engesser-hypothesis-based partial-composite (TEPC) model are developed to formulate the stability and vibration problems of columns and beams composed of any number of identical constituting layers, incorporating the effect of interlayer partial interaction imperfection. The governing differential equations of motions and boundary conditions are extracted using the extended Hamilton's energy principle, and an exact analytical

solution scheme is implemented to solve the buckling and vibration problems for different boundary conditions. As a result, efficient conversion coefficients are introduced in terms of some dimensionless group of parameters and the number of constituting layers, generalizing the well-known classical Euler- and Timoshenko buckling and vibration formulae to those of multilayer columns and beams incorporated the interlayer imperfect interaction effects. The coefficients are general in nature and are developed in terms of the “effective lengths” to capture different classical end conditions. Some important conclusions are drawn based on the presented numerical results.

2. Problem definition and fundamental assumptions

Consider a multilayer beam/column composed of N identical layers of thickness h_ℓ , width b and length L , as shown in Fig. 1. The origin of the coordinate axis z is located at the in-depth centroid of the full-composite section (cg, ∞), and the zero- x - axis is located at one end of the multilayer (along the longitudinal direction), as indicated in Fig. 1.

Also, the distance between the centroid of the i -th layer (i.e., cg, i) to that of its adjacent is denoted by $d_{i/(i+1)}$ which is obviously equal to h_ℓ due to the identical geometry of the layers. The subscript ‘ $i + 1$ ’ refers to the layer at the bottom of the i -th layer.

We employ the partial-composite theory in conjunction with both the Euler-Bernoulli- and the Timoshenko/Engesser shear models for each sub-element layer to incorporate the effect of interfacial bonding imperfection in the structural buckling and vibration analyses. The kinematics of the present partial-composite multilayer model according to the shear deformable Timoshenko/Engesser hypothesis is illustrated in Fig. 2.

Obviously, the assumed kinematics is degraded to that of the EBPC model by disregarding the shear strains γ , as well as neglecting the rotary inertia effects from the dynamic deformations.

In Fig. 2, $V_{S,i/(i+1)}$ ($i = 1, 2, 3, \dots, N-1$) is the interlayer shear force due to the partial interaction between the layers ‘ i ’ and ‘ $i + 1$ ’. Also, M_i , $N_{F,i}$ and V_i ($i = 1, 2, 3, \dots, N$) are the internal bending moment, internal axial- and shear forces acting on the i -th layer, respectively. γ is the in-plane shear strain, and φ is the rotation due to the displacements in the layered beam/column elements and the additional shear strains,

according to the Timoshenko/Engesser kinematics.

The interlayer shear force $V_{S,i/(i+1)}$ of the deformed multilayer element is correlated to the relative slip at the interface $\Delta u_{i/(i+1)}$, generated as a result of the transverse displacements of the adjacent layers by the slip modulus k based on a linear shear spring model as [85]:

$$V_{S,i/(i+1)} = k\Delta u_{i/(i+1)} = k(u_{i+1} - u_i + h_\ell w'), \quad (i = 1, 2, 3, \dots, N-1) \quad (1)$$

For the case of buckling problem, the total external axial compressive load, $P_0 = \sum_{i=1}^N P_i$, is assumed to be shared between all the layers, acting via their cross-sections’ centroid, as shown in Fig. 2. Obviously, no pre-buckling state requires that the shared load between the layers be proportional to their axial stiffnesses, i.e. in a general state,

$$P_1/EA_1 = P_2/EA_2 = \dots = P_i/EA_i = \dots = P_{N-1}/EA_{N-1} = P_N/EA_N \quad (2)$$

where P_i ($i = 1, 2, 3, \dots, N$) is the load share carried by the i -th layer. It is noteworthy that this is a realistic assumption and valid until the bifurcation moment and buckling occurrence (see Challamel and Girhammar [61]). As the layers are assumed to be identical, their material properties are the same (E_ℓ and G_ℓ are the Young’s and shear moduli of each layer). Therefore, according to the fundamental assumption by Eq. (2), the axial compressive load will be identically distributed between the layers; i.e.: $P_i = P_0/N = P_\ell$ ($i = 1, 2, \dots, N$).

The total axial stiffness, EA_0 , shear stiffness, GA_0 , the total flexural rigidity of a layered beam/column with zero interlayer interaction (non-composite), EI_0 , are thus given as

$$EA_0 = \sum_{i=1}^N EA_i = N(EA_\ell) \quad (3a)$$

$$K_s GA_0 = \sum_{i=1}^N K_s GA_i = N(K_s GA_\ell) \quad (3b)$$

$$EI_0 = \sum_{i=1}^N EI_i = N(EI_\ell) \quad (3c)$$

In Eq. (3b), K_s is the shear correction factor, a coefficient to compensate

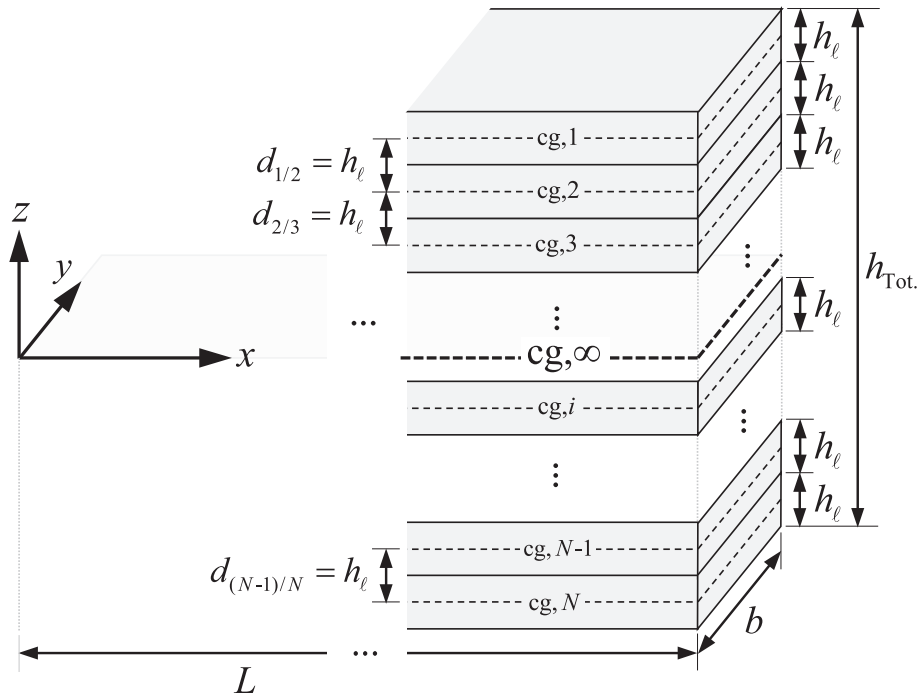


Fig. 1. Coordinate system and geometric configuration of the N -layer beam/column structural element with interfacial bonding imperfection.

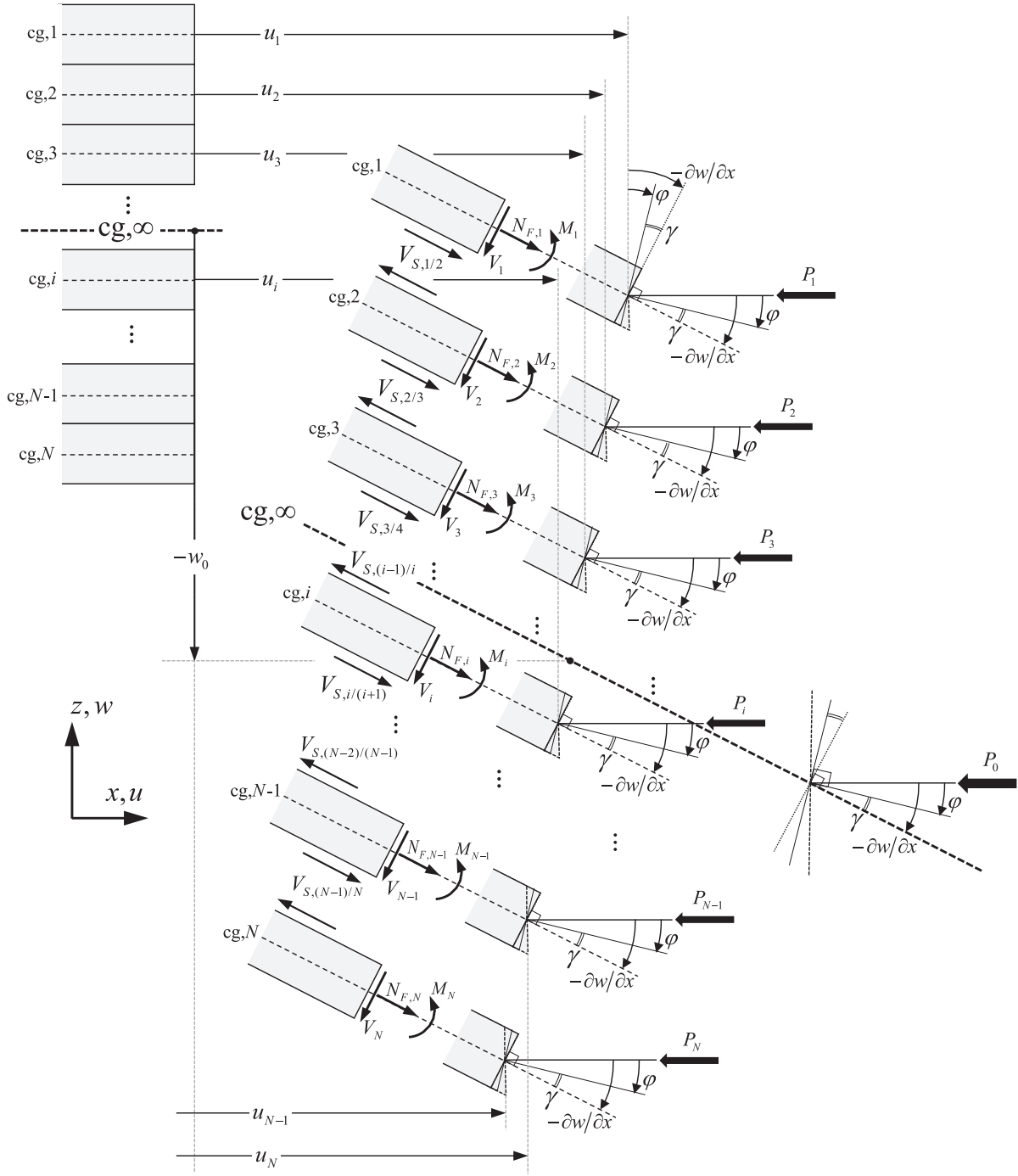


Fig. 2. Kinematics of the present partial-composite multilayer model based on the Timoshenko/Engesser hypothesis (degraded to the Euler-Bernoulli-based model by disregarding the shear strains γ and the rotary inertia).

for the error due to the assumption of constant through-depth shear strains based on first-order shear deformation kinematics and is normally taken as 5/6 for the solid rectangular cross-sectional elements [11,86]. Furthermore, I_ℓ in Eq. (3c) is the second moment of area of each individual layer. The flexural rigidity of a multilayer element with ideal/perfect bonding and full-composite interaction at its interlayers (i.e., integrated cross-section), EI_∞ , is obviously given by

$$EI_\infty = \sum_{i=1}^N (EI_i + d_{cg,i}^2 EA_i) = N^3 (EI_\ell) \quad (4)$$

Also, the mass per unit length of a layered element, as well as the mass

moment of inertia of a non-composite and full-composite beam/column element for dynamic effects are defined as

$$\rho A_0 = \sum_{i=1}^N \rho A_i = N(\rho A_\ell) \quad (5a)$$

$$\rho I_0 = \sum_{i=1}^N \rho I_i = N(\rho I_\ell) \quad (5b)$$

$$\rho I_\infty = \sum_{i=1}^N (\rho I_i + d_{cg,i}^2 \rho A_i) = N^3 (\rho I_\ell) \quad (5a)$$

where ρ is the mass density of the constituting material of the layers.

3. Multilayer partial-composite model based on the Euler-Bernoulli hypothesis

We treat the problem of buckling and vibrations of multilayer composite columns and beams with interlayer partial-interaction imperfection, composed of identical layers, first, according to an Euler-Bernoulli-kinematic-based partial-composite model and introduce simple formulae based on an exact analytical solution approach for the developed governing differential equations.

3.1. Governing differential equations and classic end conditions of the model

For the structural problem described in the previous section, the kinetic energy of the system, T , as well as the total potential energy in terms of the elastic strain energy, U_{str} , and the energy of the external buckling loads, U_{ext} , can be expressed in the form:

$$\begin{aligned}
 & (U_{str} + U_{ext})[u_1, u_2, \dots, u_i, \dots, u_{N-1}, u_N, w] \\
 &= \int_0^L \left\{ \frac{1}{2} N(EI_\ell w''^2) + \frac{1}{2} EA_\ell \sum_{i=1}^N u_i'^2 \right. \\
 & \quad \left. + \frac{1}{2} \sum_{i=1}^{N-1} k(u_{i+1} - u_i + h_\ell w')^2 \right. \\
 & \quad \left. - \frac{1}{2} N(P_\ell w^2) + P_\ell \sum_{i=1}^N u_i \right\} dx \tag{6a}
 \end{aligned}$$

$$\begin{aligned}
 & T[u_1, u_2, \dots, u_i, \dots, u_{N-1}, u_N, w] \\
 &= \int_0^L \left\{ \frac{1}{2} \rho A_\ell \sum_{i=1}^N \dot{u}_i^2 + \frac{1}{2} N(\rho A_\ell \dot{w}^2) \right\} dx \tag{6b}
 \end{aligned}$$

where the displacement components w and u_i indicate the transverse displacement of the multilayer and the axial displacement in the i -th layer, respectively. The over-script dots denote partial derivatives with respect to time t . It should be pointed out that the third energy term in Eq. (6a) is the potential energy due to the relative shear slips at the interlayers (see Eq. (1)), while the last energy term is due to the contribution of the interlayer shear slips to the energy of the external compressive loads.

Employing the extended Hamilton's energy principle [87] as

$$\delta \int_{t_1}^{t_2} (T - \Pi) dt = 0 \tag{7}$$

in which $\Pi = U_{str} + U_{ext}$ is the system's total potential energy, in conjunction with Eq. (6a,b) yields the set of governing differential equations of motion and buckling of an N -layer beam/column, incorporating the effect of each layer's longitudinal mass inertia in addition to the transverse vibration effects, in the form:

$$\begin{aligned}
 & EA_\ell u_i'' + k(u_2 - u_1 + h_\ell w') + P_\ell = \rho A_\ell \ddot{u}_i, \quad (i = 1) \\
 & \left\{ \begin{aligned} EA_\ell u_i'' + k(u_{i+1} - 2u_i + u_{i-1}) + P_\ell &= \rho A_\ell \ddot{u}_i, \\ i &\in \{2, 3, \dots, N-1\} \end{aligned} \right. \tag{8} \\
 & EA_\ell u_N'' - k(u_N - u_{N-1} + h_\ell w') + P_\ell = \rho A_\ell \ddot{u}_N, \quad (i = N) \\
 & EI_0 w^{(4)} - kh_\ell \sum_{i=1}^{N-1} (u_{i+1}' - u_i' + h_\ell w'') + (P_0 w')' + \rho A_0 \ddot{w} = 0
 \end{aligned}$$

Moreover, at any end of the column/beam element, the geometric/natural boundary conditions require the specification of:

$$\begin{aligned}
 & \text{either } \delta u_1 = 0 \quad \text{or } EA_\ell u_1' + P_\ell = 0 \\
 & \text{either } \delta u_2 = 0 \quad \text{or } EA_\ell u_2' + P_\ell = 0 \\
 & \dots \\
 & \text{either } \delta u_i = 0 \quad \text{or } EA_\ell u_i' + P_\ell = 0 \\
 & \dots \\
 & \text{either } \delta u_{N-1} = 0 \quad \text{or } EA_\ell u_{N-1}' + P_\ell = 0 \\
 & \text{either } \delta u_N = 0 \quad \text{or } EA_\ell u_N' + P_\ell = 0 \\
 & \dots \\
 & \text{either } \delta w = 0 \quad \text{or } EI_0 w'' - kh_\ell \sum_{i=1}^{N-1} (u_{i+1} - u_i + h_\ell w') + P_0 w' = 0 \\
 & \text{either } \delta w' = 0 \quad \text{or } w'' = 0 \tag{9}
 \end{aligned}$$

An exact solution scheme is implemented in the following for the buckling and vibration problems.

3.2. Exact solution approach for the buckling problem

3.2.1. Simply-supported columns

The set of boundary conditions of a layered simply-supported column according to the present Euler-Bernoulli-hypothesis based partial-composite (EBPC) model is deduced from Eq. (9) as

$$\begin{aligned}
 u_1'|_{x=0,L} = u_2'|_{x=0,L} = \dots = u_i'|_{x=0,L} = \dots = u_{N-1}'|_{x=0,L} = u_N'|_{x=0,L} = -\frac{P_0}{EA_0} \\
 w'|_{x=0,L} = w''|_{x=0,L} = 0 \tag{10}
 \end{aligned}$$

An admissible solution for three-layer simply-supported partial-composite columns, corresponding to the critical buckling mode and "exactly" satisfying all the end conditions, was proposed in [66]. An extension of the displacement field can be formulated here as follows:

$$\begin{aligned}
 & \left\{ \begin{aligned} u_i &= -\frac{P_\ell}{EA_\ell} x + U_i \cos \frac{\pi x}{L}, \\ i &\in \{1, 2, \dots, N\} \end{aligned} \right. \tag{11} \\
 & w = W \sin \frac{\pi x}{L}
 \end{aligned}$$

Evidently, the identical normal strains at both ends of the beam, based on the boundary conditions (10), gradually deviate from one layer to another at their inner points due to the shear interaction at the upper and/or bottom interfaces, resulting from the transverse displacements of the partial-composite elements (see Eq. (11)).

Substituting the shape functions (11) into Eq. (8) yields

$$\begin{aligned}
 & [1 + 1/(N\bar{k})]U_1 - U_2 - (\bar{h}/N)W = 0 \\
 & \left\{ \begin{aligned} U_{i+1} - [2 + 1/(N\bar{k})]U_i + U_{i-1} &= 0, \\ i &\in \{2, 3, \dots, N-1\} \end{aligned} \right. \tag{12a-d} \\
 & [1 + 1/(N\bar{k})]U_N - U_{N-1} + (\bar{h}/N)W = 0 \\
 & U_N - U_1 + (\bar{h}/N) \left[(N-1) + \frac{1}{12\bar{k}} \left(1 - P_0/P_{ESS}^0 \right) \right] W = 0
 \end{aligned}$$

where $P_{ESS}^0 = \pi^2 EI_0 / L^2$ is the classical Euler buckling formula for a simply-supported (SS) non-composite column (i.e., columns in which the layers are stacked on one another with zero interlayer interaction). Moreover, for generality and convenience, Eq. (12) was presented in terms of some essential dimensionless parameters in the present analyses, namely, the dimensionless thickness, \bar{h} , and dimensionless interlayer slip parameter, \bar{k} , in the form:

$$\begin{aligned} \bar{h} &= \pi \frac{h_{\text{tot}}}{L} = N\pi \frac{h_\ell}{L} \\ \bar{k} &= \frac{1}{\pi^2} \frac{kL^2}{EA_0} = \frac{1}{N\pi^2} \frac{kL^2}{EA_\ell} \end{aligned} \quad (13)$$

The set of linear second-order difference Eq. (12b) ($N - 2$ equations) is fulfilled via an exact solution in the form [88] (see Appendix A for details):

$$\begin{cases} U_i = A \cosh i\theta + B \sinh i\theta, \\ i \in \{1, 2, 3, \dots, N\} \end{cases} \quad (14)$$

Upon substitution of the solution (14) into the set of Eq. (12b), and using the standard hyperbolic angle addition/subtraction formulae, the following equation is deduced

$$\begin{aligned} \{1/(N\bar{k}) + 2(1 - \cosh\theta)\} (A \cosh i\theta + B \sinh i\theta) \\ = \{1/(N\bar{k}) + 2(1 - \cosh\theta)\} U_i = 0 \end{aligned} \quad (15)$$

The nontrivial condition for the above equation (i.e., $U_i \neq 0$) is to set:

$$\theta = \cosh^{-1} [1 + 1/(2N\bar{k})] \quad (16)$$

The θ parameter (also defined in Appendix A) obviously depends on the number of layers and the dimensionless interlayer slip parameter. Satisfaction of the remaining governing equations, i.e. Eqs. (12a,c-d) is pursued through the following nontrivial solution:

$$\begin{vmatrix} \cosh 2\theta - \left(1 + \frac{1}{N\bar{k}}\right) \cosh \theta & \sinh 2\theta - \left(1 + \frac{1}{N\bar{k}}\right) \sinh \theta & \frac{1}{N\bar{h}} \\ \left(1 + \frac{1}{N\bar{k}}\right) \cosh N\theta - \cosh(N\theta - \theta) & \left(1 + \frac{1}{N\bar{k}}\right) \sinh N\theta - \sinh(N\theta - \theta) & \frac{1}{N\bar{h}} \\ \cosh N\theta - \cosh \theta & \sinh N\theta - \sinh \theta & \frac{1}{N\bar{h}} \left[(N-1) - \frac{1}{12\bar{k}} \left(\frac{P}{P_{E,SS}^0} - 1 \right) \right] \end{vmatrix} = 0 \quad (17)$$

It is easy to show that the solution of Eq. (17) for the critical buckling load can be presented after replacing Eq. (16) and performing some manipulations in the following compact form:

$$\frac{P}{P_{E,SS}^0} = 1 + 12\bar{k} \left(N - \frac{\tanh N\theta/2}{\tanh \theta/2} \right) \quad (18)$$

where $P_{E,SS}^0 = \pi^2 EI_0/L^2$ is the classic Euler bucking formula for a non-composite column comprised of N non-interacting layers.

3.2.2. Cantilever (clamped-free) columns

For a cantilever partial-composite column composited of N layers which is built-in at its lower end and is unrestrained against lateral/shear forces at its upper end where the compressive load is applied, the boundary conditions from Eq. (9) can be extracted as

$$\begin{aligned} \text{at Clamped end } (x=0): \\ u_1|_{x=0} = u_2|_{x=0} = \dots = u_i|_{x=0} = \dots = u_{N-1}|_{x=0} = u_N|_{x=0} = 0 \\ w'|_{x=0} = 0 \\ w''|_{x=0} = 0 \end{aligned} \quad (19a-c)$$

at Free end ($x=L$):

$$\begin{aligned} u_1'|_{x=L} = u_2'|_{x=L} = \dots = u_i'|_{x=L} = \dots = u_{N-1}'|_{x=L} = u_N'|_{x=L} = \frac{P_0}{EA_0} \\ w''|_{x=L} = 0 \end{aligned} \quad (19d-f)$$

$$EI_0 w''' - kh_\ell \sum_{i=1}^{N-1} (u_{i+1} - u_i + h_\ell w) + P_0 w' \Big|_{x=L} = 0$$

The last of the above boundary equations for the column's free end (i.e., Eq. (19f)) is related to the zero-shear force condition. To treat this boundary equation, we refer to the last of the system's governing equation (8) for the buckling problem (i.e., in the absence of the time-dependent terms), and rewrite it, by expanding the series, as

$$EI_0 w^{(4)} - kh_\ell (u'_N - u'_1) + [P_0 - (N-1)kh_\ell^2] w'' = 0 \quad (20)$$

Integrating Eq. (20) once with respect to x will result in an identical equation to the boundary equation (19f) in which the integration constant must set to be zero. Recalling the boundary equations (19d,e) for the free column-end condition, the second and third terms of Eq. (20) will obviously vanish at $x=L$ and consequently, it requires that the following conditions be satisfied for a free end:

$$w^{(4)}|_{x=L} = 0 \quad (21)$$

Thus, the boundary Eq. (19f) can be replaced with Eq. (21) for a free end.

A possible buckling shape function for the columns displacement components that exactly satisfies the described cantilever columns' boundary conditions may be introduced as (see [66]):

$$\begin{cases} u_i = -\frac{P_\ell}{EA_\ell} x + U_i \sin \frac{\pi x}{2L}, \\ i \in \{1, 2, 3, \dots, N\} \end{cases} \quad (22)$$

$$w = W \left(\cos \frac{\pi x}{2L} - 1 \right)$$

Substituting the buckling shape function by Eq. (22) into the governing Eqs. (8) and using the definition of dimensionless thickness, \bar{h} , and dimensionless interlayer slip parameter, \bar{k} , from Eq. (13), yields

$$\begin{aligned} [2 + 1/(2N\bar{k})] U_1 - 2U_2 + (\bar{h}/N) W = 0 \\ \begin{cases} U_{i+1} - [2 + 1/(4N\bar{k})] U_i + U_{i-1} = 0, \\ i \in \{2, 3, \dots, N-1\} \end{cases} \\ [2 + 1/(2N\bar{k})] U_N - 2U_{N-1} - (\bar{h}/N) W = 0 \\ 2(U_N - U_1) - (\bar{h}/N) \left[(N-1) + \frac{1}{48\bar{k}} \left(1 - P_0/P_{E,CF}^0 \right) \right] W = 0 \end{aligned} \quad (23)$$

in which $P_{E,CF}^0 = \pi^2 EI_0/(4L^2)$ is the classic Euler bucking formula for a non-composite cantilever (clamped-free) column composed of N non-interacting layers.

The set of Eqs. (23b) can be fulfilled in a similar manner via the

solution approach given in Eq. (14). Introducing Eq. (14) into Eq. (23b) and performing some mathematical operations, the coefficients U_i in the displacement field (22) will be determined as

$$\begin{cases} U_i = A \cosh\{\operatorname{icosh}^{-1}[1 + 1/(8N\bar{k})]\} \\ \quad + B \sinh\{\operatorname{icosh}^{-1}[1 + 1/(8N\bar{k})]\}, \\ i \in \{1, 2, 3, \dots, N\} \end{cases} \quad (24)$$

in which A and B are two constant coefficients. Satisfying the remaining Eqs. (23a,c,d) in a nontrivial solution in conjunction with Eq. (24) will result in a determinant equation, where the solution can be represented as follows

$$\frac{P}{P_{E,CF}^0} = 1 + 12\bar{k}_e \left(N - \frac{\tanh N\theta_e/2}{\tanh\theta_e/2} \right) : \quad (25)$$

$$\theta_e = \cosh^{-1}[1 + 1/(2N\bar{k}_e)]$$

where the effective dimensionless thickness, \bar{h}_e , and interlayer slip parameter, \bar{k}_e , are defined as

$$\bar{h}_e = \pi \frac{h_{Tot.}}{L_e} = N\pi \frac{h_\ell}{L_e} \quad (26)$$

$$\bar{k}_e = \frac{1}{\pi^2} \frac{kL_e^2}{EA_0} = \frac{1}{N\pi^2} \frac{kL_e^2}{EA_\ell}$$

and $L_e = 2L$ is the “effective buckling length” for a cantilever (clamped-free) column. Obviously, $P_{E,CF}^0$ is the classic Euler buckling formula for the mentioned end conditions [42,89]:

$$P_{E,CF}^0 = \frac{\pi^2 EI_0}{L_e^2}, \quad L_e = 2L \quad (27)$$

3.2.3. Other classical boundary conditions

The solution presented in the previous subsections can be applied to other classical boundary conditions in terms of the effective buckling length. Based on Eq. (9), the set of boundary conditions for a clamped-clamped (CC) multilayer partial-composite Euler column can be given as

$$\begin{aligned} u_1|_{x=0} &= u_2|_{x=0} = \dots = u_i|_{x=0} = \dots = u_{N-1}|_{x=0} = u_N|_{x=0} = 0 \\ u'_1|_{x=L} &= u'_2|_{x=L} = \dots = u'_i|_{x=L} = \dots = u'_{N-1}|_{x=L} = u'_N|_{x=L} = -P_0/EA_0 \\ w|_{x=0,L} &= w'|_{x=0,L} = 0 \end{aligned} \quad (28)$$

and for a clamped-sliding column (CS):

$$\begin{aligned} u_1|_{x=0} &= u_2|_{x=0} = \dots = u_i|_{x=0} = \dots = u_{N-1}|_{x=0} = u_N|_{x=0} = 0 \\ u'_1|_{x=L} &= u'_2|_{x=L} = \dots = u'_i|_{x=L} = \dots = u'_{N-1}|_{x=L} = u'_N|_{x=L} = -P_0/EA_0 \\ w|_{x=0} &= w'|_{x=0,L} = \{w'' - [kh_\ell/(EI_0)](u_N - u_1)\}|_{x=L} = 0 \end{aligned} \quad (29)$$

Admissible displacement fields for the above end cases can be considered as follows [66],

For CC case:

$$\begin{cases} u_i = -\frac{P_\ell}{EA_\ell} x + U_i \sin \frac{2\pi x}{L}, \\ i \in \{1, 2, 3, \dots, N\} \end{cases} \quad (30a)$$

$$w = W \left(\cos \frac{2\pi x}{L} - 1 \right)$$

For CS case:

$$\begin{cases} u_i = -\frac{P_\ell}{EA_\ell} x + U_i \sin \frac{\pi x}{L}, \\ i \in \{1, 2, 3, \dots, N\} \end{cases} \quad (30b)$$

$$w = W \left(\cos \frac{\pi x}{L} - 1 \right)$$

It is noteworthy that the considered particular displacement solution by Es. (30a) exactly fulfills all the boundary conditions of a CC case according to Eq. (28) except the axial conditions at $x=L$ (i.e., $u'_i|_{x=L} = -P_0/EA_0$). However, as the generalized kinematic boundary conditions are fulfilled in the clamped-clamped case, an analytical solution based on the considered displacement field is still valid and yields slightly upper-bound, but accurate, buckling results compared to an exact numerical-based solution. In this regard, readers are referred to [61] for a comparative study and discussion on the buckling of two-layer CC columns when the mentioned axial natural boundary conditions are not fulfilled, in comparison with the exact numerical solutions in [55].

It should also be clarified that the proposed displacement functions by Eq. (30b) for a clamped-sliding (CS) multilayer partial-composite Euler column exactly satisfy all the boundary conditions, including the last of Eq. (29) which is related to free-shear force at the unguided sliding upper end ($x=L$). This is true and valid, as the value of axial displacement in compression at the sliding end is equal for all layers due to the geometric constraints of a sliding end while the lower end is clamped; consequently, the term $(u_N - u_1)$ in the mentioned boundary equation vanishes.

Pursuing similar solution procedure introduced in the previous subsections in conjunction with the displacement field Eqs. (30a,b) for the clamped-clamped (CC) or clamped-sliding (CS) columns reveals that the obtained buckling formulae in terms of the “effective buckling length” are still valid and applicable for different end cases ($L_e = L$ for a simply-supported (SS) or clamped-sliding (CS), $L_e = 2L$ for clamped-free (CF), and $L_e = 0.5L$ for clamped-clamped (CC)). Evidently, the solution presented in this paper is not applicable to a clamped-pinned case. However, the effective length $L_e = 0.7L$ may provide a good approximation for such a case (see Atashipour et al. [66]).

3.3. A note on the partial-composite buckling formulae

The buckling formulae in the previous sections can also be expressed in a generalized more efficient form as

$$P_E^{\text{imp.}} = \eta_{pc-0} P_E^0 \quad (31)$$

where $P_E^{\text{imp.}}$ is the critical buckling load of imperfectly-bonded layered partial-composite columns, in terms of that of the classical non-composite Euler columns, P_E^0 . Also, η_{pc-0} is a dimensionless coefficient, converting the classical Euler buckling equation for an N -layer non-composite (zero-interaction) column to that of a partial-composite (PC) column, and is given in the following exact form (see Appendix B for details):

$$\eta_{pc-0} = 1 + 12\bar{k}_e \left(N - \nu_e \frac{(1 + \nu_e + 2N\bar{k}_e)^N - (2N\bar{k}_e)^N}{(1 + \nu_e + 2N\bar{k}_e)^N + (2N\bar{k}_e)^N} \right) : \quad (32)$$

$$\nu_e = \sqrt{1 + 4N\bar{k}_e}$$

and \bar{k}_e is given by Eq. (26). Obviously, the classical Euler buckling load for layered columns with non-composite interlayer interaction is expressed as

$$P_E^0 = \frac{\pi^2 EI_0}{L_e^2} \quad (33)$$

Table 1

The buckling formulae for the Euler-Bernoulli-hypothesis-based partial-composite layered columns with a specific number of constituting layers, deduced from Eq. (32) ($\alpha = N\bar{k}_e$).

	No. of columns constituting layers (N)			
	$N = 1$	$N = 2$	$N = 3$	$N = 4$
η_{pc-0}	1	$\frac{1+8\alpha}{1+2\alpha}$	$\frac{1+9\alpha}{1+\alpha}$	$\frac{1+13\alpha+32\alpha^2}{1+4\alpha+2\alpha^2}$
$\eta_{pc-\infty}$	1	$\frac{1+8\alpha}{4+8\alpha}$	$\frac{1+9\alpha}{9+9\alpha}$	$\frac{1+13\alpha+32\alpha^2}{16+64\alpha+32\alpha^2}$
	$N = 5$	$N = 6$	$N = 7$...
η_{pc-0}	$\frac{1+12.6\alpha+25\alpha^2}{1+3\alpha+\alpha^2}$	$\frac{1+16\alpha+65\alpha^2+72\alpha^3}{1+6\alpha+9\alpha^2+2\alpha^3}$	$\frac{1+15.3\alpha+54\alpha^2+49\alpha^3}{1+5\alpha+6\alpha^2+\alpha^3}$...
$\eta_{pc-\infty}$	$\frac{1+12.6\alpha+25\alpha^2}{25+75\alpha+25\alpha^2}$	$\frac{1+16\alpha+65\alpha^2+72\alpha^3}{36+216\alpha+324\alpha^2+72\alpha^3}$	$\frac{1+15.3\alpha+54\alpha^2+49\alpha^3}{49+245\alpha+294\alpha^2+49\alpha^3}$...

where L_e is the “effective buckling length”, defined for different end conditions as described in the previous sections.

The buckling equation (31) can be redefined with respect to the buckling of perfect columns having full-composite interaction between the layers and, therefore, having fully integrated sections (i.e., perfect bonding at the interlayers). This can be represented as

$$P_E^{imp.} = \eta_{pc-\infty} P_E^{\infty} \tag{34}$$

in which the dimensionless conversion coefficient $\eta_{pc-\infty}$, is a reduction factor (taken a value between zero and unity), recasting the classical Euler buckling equation for an N -layer ideal “full-composite” column to that of a partial-composite (PC) column, and is correlated to η_{pc-0} as $\eta_{pc-\infty} = \eta_{pc-0}/N^2$.

The Euler critical buckling loads of full-composite columns in terms of the effective buckling length, L_e , are given as [42,89]:

$$P_E^{\infty} = \frac{\pi^2 EI_{\infty}}{L_e^2} \tag{35}$$

The conversion coefficient η_{pc-0} by Eq. (32) (as well as and $\eta_{pc-\infty}$) can be further simplified for any specific number of constituting layers, as presented in Table 1.

3.4. Exact solution approach for the vibration problem

A general solution can be developed for the linear vibration response of N -layer beam elements with partial-composite imperfection at the layers’ interfaces based on the EBPC model introduced in the previous sections.

The structural system’s displacements are assumed here to vary harmonically with respect to the time variable, t , using the separation of variables method, as follows

$$\begin{cases} u_i(x, t) = \tilde{u}_{i,n}(x)e^{i\omega_n t}, \\ i \in \{1, 2, \dots, N\} \end{cases} \tag{36}$$

$$w(x, t) = \tilde{w}_n(x)e^{i\omega_n t}, \quad j = \sqrt{-1}$$

where $\omega_n = 2\pi f_n$ is the n -th vibration mode’s natural angular frequency of the layered beams. Substituting Eq. (36) into the set of governing differential equations (8), in the absence of any external loads, yields

$$\begin{cases} EA_e \tilde{u}_{1,n}'' + (\rho A_e \omega_n^2 - k) \tilde{u}_{1,n} + k \tilde{u}_{2,n} + h_e k \tilde{w}_n = 0, & (i = 1) \\ \left\{ \begin{aligned} k \tilde{u}_{i+1,n} + EA_e \tilde{u}_{i,n}'' + (\rho A_e \omega_n^2 - 2k) \tilde{u}_{i,n} + k \tilde{u}_{i-1,n} = 0, \\ i = 2, 3, \dots, N-1 \end{aligned} \right. & (37) \\ EA_e \tilde{u}_{N,n}'' + (\rho A_e \omega_n^2 - k) \tilde{u}_{N,n} + k \tilde{u}_{N-1,n} - h_e k \tilde{w}_n = 0, & (i = N) \\ EI_0 \tilde{w}_n^{(4)} - kh_e \sum_{i=1}^{N-1} (\tilde{u}_{i+1,n} - \tilde{u}_{i,n} + h_e \tilde{w}_n) - \rho A_0 \omega_n^2 \tilde{w}_n = 0 \end{cases}$$

In the following, we treat the classical simply-supported end case and next generalize it to serve as a flexible solution, covering different end conditions.

With inspiration from the solution conducted in sub-section 3.2.1, an admissible displacement field for the vibration modes of a simply-supported beam that exactly satisfies the boundary constraints (10) is considered here in the form:

$$\begin{cases} \tilde{u}_{i,n} = (\tilde{A}_n \cosh i \theta_n + \tilde{B}_n \sinh i \theta_n) \cos \lambda_n x, \\ i \in \{1, 2, \dots, N\} \\ \tilde{w}_n = \tilde{W}_n \sin \lambda_n x, \quad (\lambda_n = n\pi/L) \end{cases} \tag{38}$$

and \tilde{A}_n and \tilde{B}_n are constant coefficients. The set of Eqs. (37b) can be exactly satisfied and vanish upon substitution of the proposed solution (38), if we set:

$$\theta_n = \cosh^{-1} \left[1 + \frac{1}{2Nk} (n^2 - \bar{\omega}_n^2) \right] \tag{39}$$

where the dimensionless frequency $\bar{\omega}_n$ is defined as

$$\bar{\omega}_n = \frac{1}{\pi} L \sqrt{\rho/E} \omega_n \tag{40}$$

and any other previously-defined dimensionless parameters (see Eq. (13)) are valid and applicable in this section as well.

Substituting the solution (38) in conjunction with Eq. (39) into the remaining three equations (37a,c,d), and applying a non-trivial solution by collecting the coefficients of displacement factors \tilde{A}_n , \tilde{B}_n and \tilde{W}_n will result in the following determinant equation

$$\begin{vmatrix} \cosh 2\theta_n - \left[1 + \frac{1}{N\bar{k}}(n^2 - \bar{\omega}_n^2)\right] \cosh \theta_n & \sinh 2\theta_n - \left[1 + \frac{1}{N\bar{k}}(n^2 - \bar{\omega}_n^2)\right] \sinh \theta_n & \frac{n\bar{h}}{N} \\ \left[1 + \frac{1}{N\bar{k}}(n^2 - \bar{\omega}_n^2)\right] \cosh N\theta_n - \cosh(N\theta_n - \theta_n) & \left[1 + \frac{1}{N\bar{k}}(n^2 - \bar{\omega}_n^2)\right] \sinh N\theta_n - \sinh(N\theta_n - \theta_n) & \frac{n\bar{h}}{N} \\ \cosh N\theta_n - \cosh \theta_n & \sinh N\theta_n - \sinh \theta_n & \frac{n\bar{h}}{N} \left[(N-1) + \frac{1}{12} \frac{1}{\bar{k}} \left(n^2 - \frac{3}{\bar{h}^2} (2N/n)^2 \bar{\omega}_n^2 \right) \right] \end{vmatrix} = 0 \tag{41}$$

This will result in a transcendental characteristic equation whose roots are the natural frequencies for different vibration modes as

$$1 + \left(\frac{N^2}{n^2 \bar{h}^2 \bar{k}} \bar{\omega}_n^2 - \frac{n^2}{12\bar{k}} - N \right) \frac{\tanh \theta_n / 2}{\tanh N\theta_n / 2} = 0 : \tag{42}$$

$$\theta_n = \cosh^{-1} \left[1 + \frac{1}{2N\bar{k}} (n^2 - \bar{\omega}_n^2) \right]$$

As will be demonstrated in Section 5, the effect of the beam layers' longitudinal mass inertia on the vibration of partial-composite beams is negligible in comparison with those of transverse vibration effects. Therefore, an approximate but accurate solution for the vibration frequencies can be represented in closed form as

$$\bar{\omega}_{n,E,SS} = \frac{n\bar{h}}{2\sqrt{3}N} \sqrt{n^2 + 12\bar{k} \left(N - \frac{\tanh N\theta_n / 2}{\tanh \theta_n / 2} \right)} : \tag{43}$$

$$\theta_n = \cosh^{-1} \left[1 + n^2 / (2N\bar{k}) \right],$$

($n = 1, 2, \dots$)

A remark on other classical conditions is given in Appendix C.

3.5. A note on the partial-composite vibration formulae

For generality and convenience in modal dynamic applications, we introduce the natural frequencies of a flexible N -layer partial-composite beam in the form of a modified classical Euler-Bernoulli beam vibration formula as

$$\omega_{n,E}^{Imp.} = \kappa_{pc-0} \omega_{n,E}^0, \quad (n = 1, 2, 3, \dots) \tag{44}$$

where $\omega_{n,E}^0$ is the n -th vibration mode's natural frequency of an Euler-Bernoulli beam with "zero-composite interaction" at its interlayers; i. e. [44],

Table 2

The vibrations frequency formulae for the Euler-Bernoulli's partial-composite beams composed of a specific number of constituting layers, directly deduced from Eq. (46) ($\alpha = N\bar{k}_e$).

	No. of columns constituting layers (N)			
	$N = 1$	$N = 2$	$N = 3$	$N = 4$
$\kappa_{pc-\infty}$	1	$\frac{1}{2} \sqrt{\frac{n^2 + 8\alpha}{n^2 + 2\alpha}}$	$\frac{1}{3} \sqrt{\frac{n^2 + 9\alpha}{n^2 + \alpha}}$	$\frac{1}{4} \sqrt{\frac{n^4 + 13n^2\alpha + 32\alpha^2}{n^4 + 4n^2\alpha + 2\alpha^2}}$
	$N = 5$	$N = 6$	$N = 7$...
$\kappa_{pc-\infty}$	$\frac{1}{5} \sqrt{\frac{n^4 + 12.6n^2\alpha + 25\alpha^2}{n^4 + 3n^2\alpha + \alpha^2}}$	$\frac{1}{6} \sqrt{\frac{n^6 + 16n^4\alpha + 65n^2\alpha^2 + 72\alpha^3}{(n^4 + 4n^2\alpha + \alpha^2)(n^2 + 2\alpha)}}$	$\frac{1}{7} \sqrt{\frac{n^6 + 15.3n^4\alpha + 54n^2\alpha^2 + 49\alpha^3}{n^6 + 5n^4\alpha + 6n^2\alpha^2 + \alpha^3}}$...

$$\omega_{n,E}^0 = \frac{n^2 \pi^2}{L_e^2} \sqrt{\frac{EI_0}{\rho A_0}} \tag{45}$$

and κ_{pc-0} is the conversion factor, replicating the natural frequencies of

an N -layer beam with partial-composite interaction at its constituting layers' interfaces, and is expressed in the form (similar procedure to what presented in Appendix B):

$$\kappa_{pc-0} = \sqrt{1 + \frac{12\bar{k}_e}{n^2} \left(N - \frac{c_e}{n} \frac{(n^2 + nc_e + 2N\bar{k}_e)^N - (2N\bar{k}_e)^N}{(n^2 + nc_e + 2N\bar{k}_e)^N + (2N\bar{k}_e)^N} \right)} : \tag{46}$$

$$c_e = \sqrt{n^2 + 4N\bar{k}_e}$$

where n and N are the layered element's vibration mode number and the number of layers, respectively, as indicated previously. Also, the dimensionless interlayer partial-interaction modulus \bar{k}_e is given by Eq. (26). Obviously, the effective eigenmode length, L_e , can be chosen to reflect an appropriate end case; see subsection 3.4.2. It is noteworthy that $\kappa_{pc-0} \geq 1$, and the lower-bound unity reflects a case in which the frictionless layers lay one another without any interaction.

Eq. (44) can be reformulated to capture the vibration frequencies of N -layer partial-composite beams in terms of those of the classical Euler-Bernoulli's beam with perfect bonding and full-composite interaction in between the layers, $\omega_{n,E}^\infty$, as

$$\omega_{n,E}^{Imp.} = \kappa_{pc-\infty} \omega_{n,E}^\infty, \quad (n = 1, 2, \dots) \tag{47a}$$

$$\omega_{n,E}^\infty = \frac{n^2 \pi^2}{L_e^2} \sqrt{\frac{EI_\infty}{\rho A_0}} \tag{47b}$$

It is easy to show that the conversion coefficient $\kappa_{pc-\infty}$ can be expressed as $\kappa_{pc-\infty} = \kappa_{pc-0} / N$.

For a layered beam with a specific number of constituting layers, conversion coefficients η_{pc-0} and $\eta_{pc-\infty}$ can be expressed in a simple condensed form by performing mathematical manipulations on Eq. (54), as given in Table 2.

4. Partial-composite model based on Timoshenko/Egesser hypothesis

In this section, we introduce exact buckling and vibration formulae for multilayer columns and beams that consist of any arbitrary number of layers, incorporated the interfacial bonding imperfection effects based on the partial-composite theory in conjunction with the Timoshenko/Egesser kinematic hypothesis (see Fig. 2).

4.1. Governing differential equations and classic end conditions

The structural system's total potential energy (in terms of the elastic strain energy, $U_{\text{str.}}$, and the potential energy of the external compressive buckling loads, $U_{\text{ext.}}$) and the kinetic energy, T , related to the described model in Section 2 can be defined as follows,

$$\begin{aligned} & (U_{\text{str.}} + U_{\text{ext.}})[u_1, u_2, \dots, u_i, \dots, u_{N-1}, u_N, w, \varphi] \\ &= \int_0^L \left\{ \frac{1}{2} N(EI_\ell \varphi^2) + \frac{1}{2} EA_\ell \sum_{i=1}^N u_i^2 \right. \\ & \quad \left. + \frac{1}{2} N[K_s GA_\ell (\varphi + w')^2] \right. \\ & \quad \left. + \frac{1}{2} \sum_{i=1}^{N-1} k(u_{i+1} - u_i - h_\ell \varphi)^2 \right. \\ & \quad \left. - \frac{1}{2} N(P_\ell w^2) + P_\ell \sum_{i=1}^N u_i \right\} dx \end{aligned} \quad (48a)$$

$$\begin{aligned} & T[u_1, u_2, \dots, u_i, \dots, u_{N-1}, u_N, w, \varphi] \\ &= \int_0^L \left\{ \frac{1}{2} \rho A_\ell \sum_{i=1}^N \dot{u}_i^2 + \frac{1}{2} N(\rho A_\ell \dot{w}^2) + \frac{1}{2} N(\rho I_\ell \dot{\varphi}^2) \right\} dx \end{aligned} \quad (48b)$$

which clearly includes the bending, normal, and shear strain energies of each layer, the translational and rotational dynamic energies of all layers, the energy associated with the work done by the axial compressive external loads for both in-plane- and transverse displacements, as well as the energy stored at the layers' interfaces corresponding to the imperfect bonding between the layers and their subsequent partial interaction behavior. Also, K_s is the shear correction factor, as mentioned earlier (see Section 2). It is noteworthy that any other parameters and functions in Eq. (48) are defined in Sections 2 and 3.1.

Applying the extended Hamilton's variational energy principle to Eqs. (48a,b), the set of $N+2$ governing differential equations of the model are obtained in the form:

$$\begin{aligned} & EA_\ell u_1'' + k(u_2 - u_1 - h_\ell \varphi) + P_\ell = \rho A_\ell \ddot{u}_1, \quad (i = 1) \\ & \begin{cases} EA_\ell u_i'' + k(u_{i+1} - 2u_i + u_{i-1}) + P_\ell = \rho A_\ell \ddot{u}_i, \\ i \in \{2, 3, \dots, N-1\} \end{cases} \\ & EA_\ell u_N'' - k(u_N - u_{N-1} - h_\ell \varphi) + P_\ell = \rho A_\ell \ddot{u}_N, \quad (i = N) \\ & EI_0 \varphi'' + h_\ell k \sum_{i=1}^{N-1} (u_{i+1} - u_i - h_\ell \varphi) - K_s GA_0 (\varphi + w') = \rho I_0 \ddot{\varphi} \\ & K_s GA_0 (\varphi + w')' - (P_0 w')' = \rho A_0 \ddot{w} \end{aligned} \quad (49)$$

and at any end of the partial-composite beam, the boundary conditions require the specification of:

$$\begin{aligned} & \text{either } \delta u_1 = 0 \quad \text{or } EA_\ell u_1' + P_\ell = 0 \\ & \text{either } \delta u_2 = 0 \quad \text{or } EA_\ell u_2' + P_\ell = 0 \\ & \dots \\ & \text{either } \delta u_i = 0 \quad \text{or } EA_\ell u_i' + P_\ell = 0 \\ & \dots \\ & \text{either } \delta u_{N-1} = 0 \quad \text{or } EA_\ell u_{N-1}' + P_\ell = 0 \\ & \text{either } \delta u_N = 0 \quad \text{or } EA_\ell u_N' + P_\ell = 0 \\ & \text{either } \delta w = 0 \quad \text{or } K_s GA_0 (\varphi + w') - P_0 w' = 0 \\ & \text{either } \delta \varphi = 0 \quad \text{or } \varphi' = 0 \end{aligned} \quad (50)$$

In the following, a generalized solution approach is implemented to the model's governing equations with application to both stability, and modal dynamic and vibration problems.

4.2. Exact solution approach for the buckling problem

It can be shown that the concept of the effective length is valid here analogously to what was presented in the previous sections based on EBPC hypothesis. Thus, for the generality of the formulation and brevity, we proceed with the simply-supported case with the effective length L_e . From Eq. (50), it can be deduced that the boundary conditions related to a simply-supported (SS) case are given as

$$\begin{aligned} u_1'|_{x=0,L} = u_2'|_{x=0,L} = \dots = u_i'|_{x=0,L} = \dots = u_{N-1}'|_{x=0,L} = u_N'|_{x=0,L} = -\frac{P_0}{EA_0} \\ w|_{x=0,L} = \varphi'|_{x=0,L} = 0 \end{aligned} \quad (51)$$

A set of admissible inverse solutions, which capture the critical buckling mode and exactly satisfy all the end conditions (51), can be considered in terms of the effective length L_e , as

$$\begin{aligned} & \begin{cases} u_i = -\frac{P_\ell}{EA_\ell} x + U_i \cos \frac{\pi x}{L_e}, \\ i = 1, 2, \dots, N \end{cases} \\ & \varphi = \Phi \cos \frac{\pi x}{L_e} \\ & w = W \sin \frac{\pi x}{L_e} \end{aligned} \quad (52)$$

Substituting the above set of shape functions into Eqs. (49) in the absence of dynamic terms, and using some effective dimensionless group of parameters yields

$$\begin{aligned} & [1 + 1/(N\bar{k}_e)]U_1 - U_2 + (h_\ell \Phi) = 0 \\ & \begin{cases} U_{i+1} - [2 + 1/(N\bar{k}_e)]U_i + U_{i-1} = 0, \\ i = 2, 3, \dots, N-1 \end{cases} \\ & [1 + 1/(N\bar{k}_e)]U_N - U_{N-1} - (h_\ell \Phi) = 0 \\ & (U_N - U_1) - \left[(N-1) + \frac{1}{12\bar{k}_e} + N^2 K_s \frac{\bar{G}}{h_e^2 \bar{k}_e} \right] (h_\ell \Phi) - NK_s \frac{\bar{G}}{h_e \bar{k}_e} W = 0 \\ & 12N^3 K_s \frac{\bar{G}}{h_e} (h_\ell \Phi) + \left(12N^2 K_s \frac{\bar{G}}{h_e} - \frac{P_0}{P_{E,e}^0} \right) W = 0 \end{aligned} \quad (53)$$

where the dimensionless thickness, \bar{h}_e , and dimensionless interlayer slip parameter, \bar{k}_e , are given by Eq. (26), and the dimensionless shear

modulus $\bar{G} = G/E$.

It can be proven that the set of governing Eqs. (53b) can be exactly satisfied if we set the axial displacement coefficients U_i in Eq. (52) to be:

$$\begin{cases} U_i = \text{Acosh}\{\text{icosh}^{-1}[1 + 1/(2N\bar{k}_e)]\} \\ \quad + \text{Bsinh}\{\text{icosh}^{-1}[1 + 1/(2N\bar{k}_e)]\}, \\ \quad i \in \{1, 2, 3, \dots, N\} \end{cases} \quad (54)$$

Satisfying the remaining Eqs. (53a,c-e) through a non-trivial solution for the coefficients of the displacement components vector $[A, B, \Phi, W]^T$, after substitution of the solution (54), will result in the following determinant-form characteristic equation:

$$\begin{vmatrix} \cosh 2\theta_e - \left(1 + \frac{1}{N\bar{k}_e}\right) \cosh \theta_e & \sinh 2\theta_e - \left(1 + \frac{1}{N\bar{k}_e}\right) \sinh \theta_e & -1 & 0 \\ \left(1 + \frac{1}{N\bar{k}_e}\right) \cosh N\theta_e - \cosh(N\theta_e - \theta_e) & \left(1 + \frac{1}{N\bar{k}_e}\right) \sinh N\theta_e - \sinh(N\theta_e - \theta_e) & -1 & 0 \\ \cosh N\theta_e - \cosh \theta_e & \sinh N\theta_e - \sinh \theta_e & -\left(N^2 K_s \frac{\bar{G}}{h_e \bar{k}_e} + N + \frac{1}{12\bar{k}_e} - 1\right) & -NK_s \frac{\bar{G}}{h_e \bar{k}_e} \\ 0 & 0 & 12N^3 K_s \frac{\bar{G}}{h_e} & \left(12N^2 K_s \frac{\bar{G}}{h_e} - \frac{P}{P_{E,e}^0}\right) \end{vmatrix} = 0 \quad (55)$$

where θ_e is defined by the last of Eq. (25). It can be shown that the exact solution of the characteristic Eq. (55) for the critical buckling load of an N -layer partial-composite Timoshenko/Engesser column can be presented in a compact form as

$$\frac{P}{P_{E,e}^0} = \frac{\left(12N^2 K_s \frac{\bar{G}}{h_e}\right) \left[1 + 12\bar{k}_e \left(N - \frac{\tanh N\theta_e/2}{\tanh \theta_e/2}\right)\right]}{\left(12N^2 K_s \frac{\bar{G}}{h_e}\right) + \left[1 + 12\bar{k}_e \left(N - \frac{\tanh N\theta_e/2}{\tanh \theta_e/2}\right)\right]} \quad (56)$$

in which the equivalent dimensionless thickness \bar{h}_e and interfacial slip modulus \bar{k}_e are defined by Eq. (26), and the parameter θ_e is given by the last of Eq. (25).

4.3. A note on the partial-composite buckling formulae based on Timoshenko/Engesser partial-composite (TEPC) model

The buckling formulae introduced in the previous section for the N -layer columns with bonding imperfection at their interlayers, can be expressed in a simple efficient form as

$$P_T^{\text{imp.}} = \psi_{T-E} \eta_{pc-0} P_E^0 : \quad P_E^0 = \pi^2 EI_0 / L_e^2 \quad (57)$$

where $P_T^{\text{imp.}}$ is the critical buckling loads of a Timoshenko/Engesser-based multilayer columns with imperfect bonding at their layers' interfaces; ψ_{T-E} is a coefficient enhancing the previously developed Euler-

based buckling formula of an N -layer partial-composite column to that of shear deformable TEPC model. Rearranging Eq. (56) from the previous section, the coefficient ψ_{T-E} can be represented in a simple form as

$$\psi_{T-E} = \left[1 + \frac{\eta_{pc-0}}{12N^2 K_s \bar{G}}\right]^{-1} \quad (58)$$

where

$$G^* = \bar{G}/\bar{h}_e^2 = \frac{1}{\pi^2} \frac{G}{E} \frac{L_e^2}{h_{\text{Tot}}^2} \quad (59)$$

As described in Section 3.3, the dimensionless coefficient η_{pc-0} in the

above equations converts the classical Euler buckling formula for an N -layer non-composite (zero-interaction between the layers) column (i.e., $P_E^0 = \pi^2 EI_0 / L_e^2$) to that of a partially-composite (PC) column. It is reminded that the definition of the factor η_{pc-0} is given by Eq. (32) (see also Table 1 in Section 3.3). For the definition of the dimensionless parameters \bar{h}_e and \bar{k}_e in terms of the "effective buckling length" L_e , (capturing different end conditions as described in Sections 3.2), see Eq. (26). Moreover, the shear-to-Young's modulus ratio $\bar{G} = G/E$.

The simple buckling equation (57) can also be redefined with respect to the buckling of perfect columns with full-composite interaction at the interlayers as

$$P_E^{\text{imp.}} = \psi_{T-E} \eta_{pc-\infty} P_E^{\infty} : \quad P_E^{\infty} = \pi^2 EI_{\infty} / L_e^2 \quad (60)$$

As described in Section 3.3, the dimensionless coefficient $\eta_{pc-\infty}$ converts the classical Euler buckling equation for an N -layer "full-composite" column to that of a partial-composite (PC) column and is given as $\eta_{pc-\infty} = \eta_{pc-0} / N^2$.

4.4. Exact solution approach for the vibration problem

An exact analytical solution is developed here for the linear vibration problem of N -layer beams with interlayer partial interaction imperfection based on the previously developed TEPC model in Section 4.1. Assuming harmonic motions, the displacement- and rotation components of the structural system can be described as

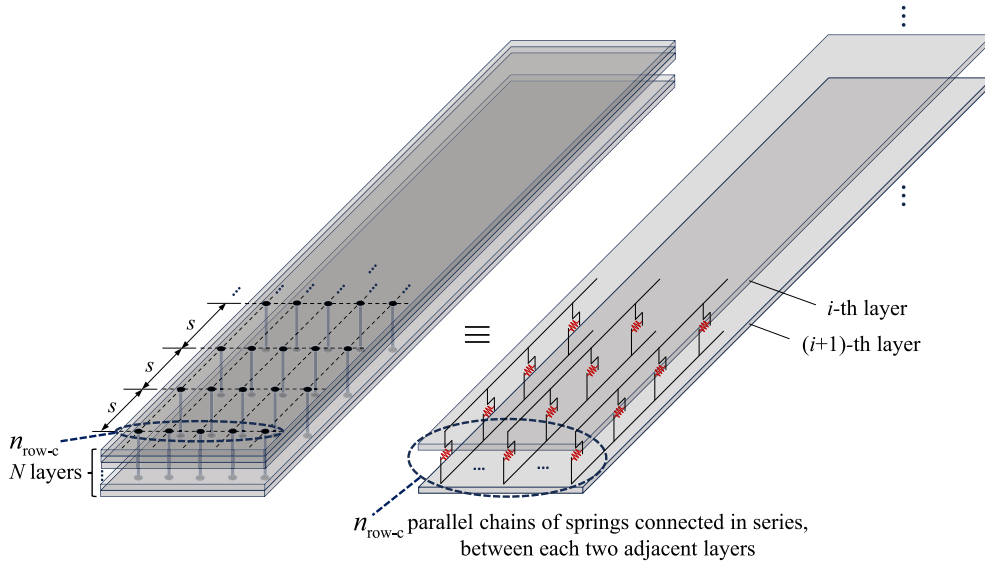


Fig. 3. The parallel rows of mechanical connectors are modeled here as parallel chains of shear springs connected in series between each pair of adjacent stacked layers.

Table 3

The imperfect partial-composite (interlayer slip) modulus, measured in [92] for three different connector materials, and via two different approaches: the direct double shear joint test (k_{Direct}), and the beam test method (k_{BT}).

Connector	k_{Direct}	k_{BT}
Rubber	3.62 MPa	4.83 MPa
Polyethylene	18.96 MPa	26.2 MPa
Nylon	620.53 MPa	1034.2 MPa

$$\begin{cases} u_i(x, t) = \tilde{u}_{i,n}(x)e^{j\omega_n t}, \\ i = 1, 2, \dots, N \end{cases} \quad (61)$$

$$\begin{aligned} \varphi(x, t) &= \tilde{\varphi}_n(x)e^{j\omega_n t}, \\ w(x, t) &= \tilde{w}_n(x)e^{j\omega_n t}, \quad j = \sqrt{-1} \end{aligned}$$

in which $\omega_n = 2\pi f_n$ is obviously the n -th vibration mode's natural angular frequency of the beam. Substituting Eq. (61) into the governing equations (49), in the absence of the external axial compressive loads yields

Table 4

Comparison of the fundamental natural frequencies ($f = \omega/(2\pi)$ [Hz]) of a three-layer partial-composite beam made of aluminum layers, with three different types of discrete mechanical connectors, predicted via the present approaches ($N = 3$: three-layer; $n = 1$: fundamental frequency) and those experimentally measured from vibration tests, reported in [92].

Approach	Connectors material		
	Rubber	Polyethylene	Nylon
Vibration test [92]	5.35 ± 0	7.25 ± 2	12.9 ± 1
Present ($f_{n,E}^{\text{imp}}(k_{\text{Direct}})$) * [Diff (%)] †	5.30 [-1.0 %]	6.68 [-7.8 %]	13.25 [2.7 %]
Present ($f_{n,E}^{\text{imp}}(k_{\text{BT}})$) * [Diff (%)] †	5.43 [1.4 %]	7.17 [-1.0 %]	13.73 [6.4 %]
Present ($f_{n,T}^{\text{imp}}(k_{\text{Direct}})$) ** [Diff (%)] †	5.30 [-1.0 %]	6.68 [-7.8 %]	13.25 [2.7 %]
Present ($f_{n,T}^{\text{imp}}(k_{\text{BT}})$) ** [Diff (%)] †	5.43 [1.4 %]	7.17 [-1.0 %]	13.73 [6.4 %]

* Euler-Bernoulli-based partial-composite (EBPC) model (Eq. (44)).

** Timoshenko/Engesser-based partial-composite (TEPC) model (Eq. (67)).

† Percentage discrepancy relative to the test data: |(present - test data [92])/test data [92]| × 100(%).

$$\begin{aligned} EA_\ell \tilde{u}''_{1,n} + (\rho A_\ell \omega_n^2 - k) \tilde{u}_{1,n} + k \tilde{u}_{2,n} - h_\ell k \tilde{\varphi}_n &= 0 \\ \left\{ \begin{aligned} k \tilde{u}_{i+1,n} + EA_\ell \tilde{u}''_{i,n} + (\rho A_\ell \omega_n^2 - 2k) \tilde{u}_{i,n} + k \tilde{u}_{i-1,n} &= 0, \\ i = 2, 3, \dots, N-1 \end{aligned} \right. \\ EA_\ell \tilde{u}''_{N,n} + (\rho A_\ell \omega_n^2 - k) \tilde{u}_{N,n} + k \tilde{u}_{N-1,n} + h_\ell k \tilde{\varphi}_n &= 0 \\ EI_0 \tilde{\varphi}_n'' + (\rho I_0 \omega_n^2 - K_s GA_0) \tilde{\varphi}_n + h_\ell k \sum_{i=1}^{N-1} (\tilde{u}_{i+1,n} - \tilde{u}_{i,n} - h_\ell \tilde{\varphi}_n) - K_s GA_0 \tilde{w}'_n &= 0 \\ K_s GA_0 (\tilde{\varphi}_n + \tilde{w}'_n)' + \rho A_0 \omega_n^2 \tilde{w}_n &= 0 \end{aligned} \quad (62)$$

In the following, we treat the vibration problem of the layered beam element with the classical simply-supported end conditions, and next, generalize the solution to be served for different end conditions.

Similar to the previous solutions, we conduct a generalized vibration solution in terms of the effective length to cover different classical end conditions. A set of admissible shape functions for the displacement-field components of a vibrating simply-supported beam, that exactly satisfies the boundary conditions (51), is considered here as

$$\begin{cases} \tilde{u}_{i,n} = \left(\tilde{A}_n \cosh i \theta_{n,e} + \tilde{B}_n \sinh i \theta_{n,e} \right) \cos \lambda_{n,e} x, \\ i = 1, 2, \dots, N \end{cases} \quad (63)$$

$$\tilde{\varphi}_n = \tilde{\Phi}_n \cos \lambda_{n,e} x$$

$$\tilde{w}_n = \tilde{W}_n \sin \lambda_{n,e} x, \quad \lambda_{n,e} = n\pi/L_e$$

Also, \tilde{A}_n and \tilde{B}_n are constant coefficients of the axial displacements of the beam's n -th vibration mode, and $\tilde{\Phi}_n$ and \tilde{W}_n are those for the rotations and transverse displacements, respectively. The set of Eqs. (62b) vanishes upon substitution of the solution (63), if we set: $\theta_{n,e} = \cosh^{-1} [1 + (n^2 - \bar{\omega}_n^2)/(2N\bar{k}_e)]$. The dimensionless frequency, $\bar{\omega}_n$, is defined according to Eq. (40). It is noteworthy that any other previously defined dimensionless parameters are also valid and applicable here. Satisfying the remaining four differential equations (62a,c-e) through substitution of the defined displacement and rotation relationships (63) and using the definition of $\theta_{n,e}$ in the form of a non-trivial solution yields:

$$\begin{vmatrix} \left[\frac{1}{N\bar{k}_e} (\bar{\omega}_n^2 - n^2) - 1 \right] \cosh \theta_{n,e} + \cosh 2\theta_{n,e} & \left[\frac{1}{N\bar{k}_e} (\bar{\omega}_n^2 - n^2) - 1 \right] \sinh \theta_{n,e} + \sinh 2\theta_{n,e} & -1 & 0 \\ \cosh(N\theta_{n,e} - \theta_{n,e}) + \left[\frac{1}{N\bar{k}_e} (\bar{\omega}_n^2 - n^2) - 1 \right] \cosh N\theta_{n,e} & \sinh(N\theta_{n,e} - \theta_{n,e}) + \left[\frac{1}{N\bar{k}_e} (\bar{\omega}_n^2 - n^2) - 1 \right] \sinh N\theta_{n,e} & 1 & 0 \\ \cosh N\theta_{n,e} - \cosh \theta_{n,e} & \sinh N\theta_{n,e} - \sinh \theta_{n,e} & \frac{1}{12\bar{k}_e} (\bar{\omega}_n^2 - n^2) - \frac{K_s \bar{G}}{h_e \bar{k}_e} N^2 - N + 1 & -\frac{K_s \bar{G}}{\bar{k}_e h_e} nN \\ 0 & 0 & -\frac{K_s \bar{G}}{\bar{k}_e h_e} nN & \frac{1}{\bar{k}_e} (\bar{\omega}_n^2 - K_s \bar{G} n^2) \end{vmatrix} = 0 \quad (64)$$

Rearranging the above determinant equation and performing some algebraic operations, the following exact vibration characteristic equation is obtained for the natural frequencies of the multilayer partial-composite beams based on the shear deformable TEPC model:

$$1 + \frac{5}{6} \left(\frac{6N^2 K_s \bar{\omega}^2}{5\bar{k}_e (n^2 K_s \bar{h}_e^2 - \bar{\omega}^2 / G^*)} - \frac{N}{5} \cosh \theta_{n,e} - N \right) \frac{\tanh \theta_{n,e} / 2}{\tanh N\theta_{n,e} / 2} = 0 :$$

$$\theta_{n,e} = \cosh^{-1} \left[1 + \frac{1}{2N\bar{k}} (n^2 - \bar{\omega}_n^2) \right] \quad (65)$$

Apparently, due to the nonlinearity of Eq. (65), it is mathematically difficult to present a closed-form solution. However, the statement regarding the negligible effect of the constituting layers' longitudinal mass inertia on the natural frequencies and vibration behavior of partial-

composite beams in the previous sections is valid. Therefore, an approximate but accurate vibration formula based on the TEPC model can be deduced, similar to what presented for the Euler-based partial-composite beams in the previous sections, as follows,

$$\bar{\omega}_{n,T,e} = \frac{n\bar{h}_e}{\sqrt{\frac{1}{K_s G^*} + \frac{N^2}{\bar{k}_e} \left[\frac{1}{6} N(5 + \cosh \theta_{n,e}) - \frac{\tanh(N\theta_{n,e}/2)}{\tanh(\theta_{n,e}/2)} \right]^{-1}}}, \quad (n = 1, 2, \dots) \quad (66)$$

in which $\theta_{n,e} = \cosh^{-1} [1 + n^2/(2N\bar{k}_e)]$.

4.5. Partial-composite vibration formulae based on the TEPC model

The formulae developed in the previous section for the vibration modes' frequencies of N -layer shear deformable beams having partial interaction imperfections at their interlayers can be rearranged and

presented in a simple efficient form as

$$\omega_{n,T}^{\text{imp}} = \zeta_{T-E} \kappa_{pc-0} \omega_{n,E}^0, \quad (n = 1, 2, 3, \dots) \quad (67)$$

where $\omega_{n,T}^{\text{imp}}$ is the n -th mode's natural frequency of the imperfectly-bonded layered beam element based on the established Timoshenko/Engesser N -layer partial-composite model. While the coefficient κ_{pc-0} (given by Eq. (46), also Table 2) converts the classical Euler-Bernoulli vibration formula for an N -layer non-composite (zero-interaction between the layers) beam (i.e., $\omega_{n,E}^0 = (n^2 \pi^2 / L_e^2) \sqrt{EI_0 / (\rho A_0)}$) to that for a partially-composite (PC) beam, as discussed in Section 3.5, the factor ζ_{T-E} enhances it to that based on the shear deformable TEPC model. Utilizing Eq. (66), ζ_{T-E} can be represented in the following simple form:

Table 5

Comparison of the first six natural frequencies ($f = \omega / (2\pi)$ [Hz]) of a cantilever two-layer beam (CF end conditions) made of glass layers bonded together by the polyvinyl butyral (PVB) elastomeric polymer, predicted via the present approaches ($N = 2$: three-layer; $n = 1, 2, \dots, 6$; the first six frequencies).

Approach	Mode sequence					
	1st	2nd	3rd	4th	5th	6th
GEM * [93]	65.02	299.65	750.35	1405.44	2279.31	3370.18
FEM ** [94]	64.93	299.31	749.73	1404.53	2277.97	3368.32
Present ($f_{n,E}^{\text{imp}}$) †	62.55 [3.7 %]	291.05 [2.8 %]	736.94 [1.7 %]	1398.41 [0.4 %]	2278.48 [0.0 %]	3377.89 [0.3 %]
Present ($f_{n,T}^{\text{imp}}$) ††	62.52 [3.7 %]	290.96 [2.8 %]	736.44 [1.8 %]	1396.68 [0.5 %]	2273.96 [0.2 %]	3368.04 [0.0 %]

† EBPC model (Eq. (44)); [% diff.] w.r.t. FEM [94] are given in parentheses.

†† TEPC model (Eq. (67)); [% diff.] w.r.t. FEM [94] are given in parentheses.

* Galerkin element method.

** Finite element method.

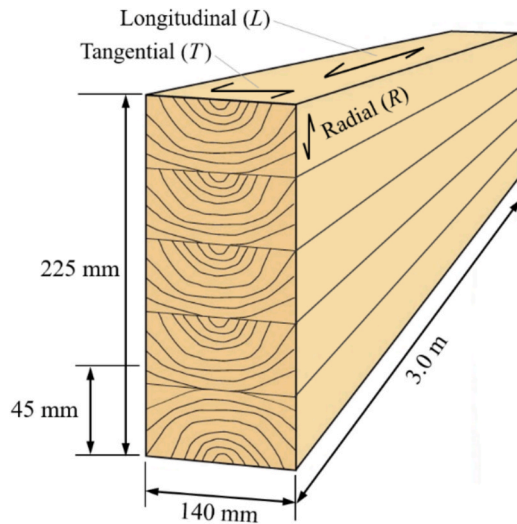


Fig. 4. Geometrical configuration and dimensions of the Swedish glued laminated timber (glulam) GL30 composed of 5 orthotropic lamellae (grain/fiber orientation along the longitudinal direction). The directional material properties, given in Table 6, are based on the illustrated: Longitudinal (L), Radial (R), and Tangential (T) orientations.

Table 6

Material properties (mean value) of the glulam GL30c [97]. The values used to represent each of the constituting lamellae based on the developed theoretical approach are $E_\ell = E_L$ and $G_\ell = G_{LR}$.

	Glulam GL30c (L:1, T:2, R:3)*		
Elastic modulus (N/mm ²)	$E_L = 13000$	$E_T = 300$	$E_R = 300$
Shear modulus (N/mm ²)	$G_{RL} = 650$	$G_{TL} = 650$	$G_{TR} = 650$
Poisson's ratio	$\nu_{RL} = 0.06$	$\nu_{TL} = 0.06$	$\nu_{TR} = 0.4$

* Material property directions are illustrated in Fig. 4.

$$\zeta_{T-E} = \frac{1}{\sqrt{1 + \frac{n^2 \kappa_{pc}^2}{12N^2 K_\ell G}}} \quad (68)$$

in which the dimensionless shear-effect parameter G^* is defined by Eq. (59) in terms of the effective length L_e , capturing different end cases (see Appendix C). It is obvious from Eq. (68) that $\zeta_{T-E} \leq 1$ (equals unity when the shear rigidity approaches infinity), meaning that the natural fre-

quencies of the layered beams predicted from the TEPC model are slightly lower than those based on the EBPC model due to the shear rigidity and, consequently, higher stiffness of the layered structures based on the EBPC theory.

5. Numerical results

In this section, numerical results and discussion are conducted based on the developed Euler-Bernoulli- (EBPC) and Timoshenko/Engesser-based partial-composite (TEPC) models and the introduced solutions for the problems of buckling and vibrations of multilayer columns/beams having bonding imperfection at their layers' interfaces. The numerical results are presented in a dimensionless format based on the group of dimensionless parameters defined in Section 4 for the sake of their generality. Also, a comprehensive comparative study is carried out and the validity and reliability of the approach is verified.

5.1. A note on methods for determining the partial-composite modulus

An accurate determination of the partial-composite/slip modulus k is essential to accurately predict and analyze the vibration and buckling results and behavior of imperfect partial-composite structural elements. This can be pursued via the known standard experimental approaches such as the double shear joint test, full-scale beam three-point bending test and comparison with the static partially composite beam theory (see [41]), etc. Alternatively, simple conventional formulae may be used; e.g. for the partial adhesive bonding layer [90]:

$$k = G_{adh} \frac{b}{h_{adh}} \quad (69)$$

in which G_{adh} and h_{adh} are the shear modulus and the thickness of the adhesive layer, respectively, and b is the width of the layered element. Eq. (69) can be accommodated with a correction coefficient of (A_{eff}/A_{int}) , where A_{eff} is the effective area of interlayer bonding, and $A_{int} = bL$ indicates a full interlayer area. Obviously, in the case of the full interlayer area covered by the adhesive layer, the partial adhesive ratio A_{eff}/A_{int} equals unity. For the case of discrete mechanical connectors, the partial-composite modulus can be calculated as [91]:

$$k = \frac{n_{row} - cK}{s} \quad (70)$$

where $n_{row} - c$ is the number of parallel rows of connectors along the longitudinal direction of a structural element, and s is the spacing be-

Table 7

The first five natural frequencies (Hz) of the partial-composite glulam GL30c beams (composed of five orthotropic lamellas) for different values of the interlayer interaction modulus, k , –ranging from zero interaction (non-composite) to perfectly-bonded (full-composite) condition. The results obtained from both the established Euler-Bernoulli-hypothesis-based (EBPC) and the Timoshenko/Engesser-based partial-composite (TEPC) model are compared with corresponding 3-D finite element analysis (FEA) results, using Abaqus CAE software (Percentage discrepancy has been calculated for any of the EBPC and TEPC cases relative to the corresponding 3-D FEA results).

Interlayer Interaction	Approach	Mode sequence				
		1st	2nd	3rd	4th	5th
$k \rightarrow 0$	EBPC [%Diff.]	12.466 [2.1 %]	49.865 [2.6 %]	112.20 [3.4 %]	199.46 [4.6 %]	311.66 [6.1 %]
	TEPC [%Diff.]	12.439 [1.9 %]	49.428 [1.7 %]	110.02 [1.4 %]	192.73 [1.0 %]	295.67 [0.7 %]
	3-D FEA	12.199	48.576	108.45	190.67	293.60
$k = 10 \text{ MPa}^*$	EBPC [%Diff.]	17.695 [1.4 %]	56.053 [2.5 %]	118.63 [3.6 %]	205.99 [4.8 %]	318.24 [6.4 %]
	TEPC [%Diff.]	17.617 [0.9 %]	55.435 [1.4 %]	116.07 [1.4 %]	198.60 [1.1 %]	301.27 [0.8 %]
	3-D FEA	17.448	54.633	114.46	196.37	298.87
$k = 10^2 \text{ MPa}$	EBPC [%Diff.]	35.802 [1.8 %]	91.533 [3.1 %]	163.42 [4.5 %]	255.92 [5.9 %]	371.18 [7.7 %]
	TEPC [%Diff.]	35.163 [0.1 %]	88.911 [0.2 %]	156.90 [0.3 %]	242.15 [0.2 %]	345.00 [0.1 %]
	3-D FEA	35.135	88.707	156.38	241.44	344.52
$k = 10^3 \text{ MPa}$	EBPC [%Diff.]	56.390 [4.4 %]	182.80 [10.9 %]	332.59 [15.4 %]	493.60 [18.5 %]	665.90 [21.1 %]
	TEPC [%Diff.]	53.991 [<0.1 %]	164.24 [0.3 %]	286.12 [0.7 %]	412.02 [1.0 %]	542.46 [1.3 %]
	3-D FEA	53.995	164.79	288.14	416.33	549.77
$k \rightarrow \infty$	EBPC [%Diff.]	62.331 [5.4 %]	249.33 [20.0 %]	560.98 [40.6 %]	997.30 [65.1 %]	1558.3 [91.8 %]
	TEPC [%Diff.]	59.135 [<0.1 %]	207.47 [0.2 %]	396.74 [0.5 %]	598.52 [0.9 %]	801.94 [1.3 %]
	3-D FEA	59.114	207.85	398.92	604.19	812.48

tween two adjacent connectors in a row, as illustrated in Fig. 3. K is the slip modulus of a single connector and can be determined experimentally via the double shear joint test or, for design purposes, using relevant standards (e.g., K_{ser} : the slip modulus in serviceability limit state (SLS) or K_u : the slip modulus in ultimate limit state (ULS), for a timber structural elements design according to Eurocode 5 standard).

It should be clarified that as the present research has focused on the developed imperfect partial-composite models and solutions for the buckling and vibrations of multilayer column/beam elements, the study of the partial-composite/slip modulus and research on its determination falls outside the scope of the present article.

5.2. Comparative results and validation

To demonstrate the validity, reliability, and high accuracy of the established analyses and solutions, as well as the resultant introduced simple buckling- and vibration formulae, a comprehensive comparative study is conducted. Comparisons are provided with both available relevant numerical and experimental data in the literature.

Henghold [92] performed vibration tests on a three-layer simply-supported beam having imperfect partial-composite interaction between the layers via some discrete mechanical connectors. The beam was of 1778 mm (70 in.) span length (total length 1828 mm \equiv 72 in.) and 101.6 mm (4 in.) width, composed of the three identical layers, each of thickness 6.50 mm (0.256 in.) from aluminum with Young's modulus 73.08 GPa (10.6×10^6 lb/in.²). The average weight of each layer was reported to be 3.277 Kg; therefore, the mass density $\rho_\ell = 2712$ Kg/m³. Two rows of connectors made of rubber, low-density polyethylene, and nylon, each of a nominal diameter of 9.13 mm (23/63 in.) with a spacing of 50.8 mm (2 in.) for all cases, except for the nylon connectors 101.6 mm (4 in.), were used. For details on the test procedure and equipment, readers are referred to [92]. The partial-composite moduli were measured in [92] based on two different experimental methods: (1) the

direct double shear joint test (k_{Direct}), and (2) the beam test method (k_{BT}); see the results in Table 3.

Despite the considerable difference between the measured moduli based on the two approaches, it is shown that the discrepancy effect on the predicted natural frequencies based on the present approach is small.

Table 4 shows a comparison of the fundamental natural frequencies predicted on the basis of the introduced Euler-based- (EBPC) and Timoshenko/Engesser-based partial-composite (TEPC) analysis approaches in the present study with those reported in [92] based on the vibration test measurements. It is evident from Table 4 that there is a good agreement between the predicted fundamental natural frequencies and the corresponding test results for all cases, confirming the validity and reliability of the introduced approach.

It can be observed that regardless of the method used to determine the partial-composite modulus k , the highest percentage discrepancy between the vibration test results and predicted values does not exceed 1.4 %, 7.8 %, and 6.4 % for the partial-composite beams with rubber, polyurethane, and nylon connectors, respectively. It can also be seen from Table 4 that, regardless of the type of connectors and their applied geometric characteristics (e.g. spacing intervals), the predicted results based on k_{Direct} are slightly lower than those predicted on the basis of k_{BT} for the interlayer interaction modulus. It can also be deduced from Table 4 that the predicted results from the TEPC model coincide with those from the EBPC model, confirming that the effect of shear deformations on the beam's flexural rigidity is negligible. This is evidently due to the large length-to-layer thickness ratio of the tested beam ($L/h_\ell = 273 \gg 10$) on the one hand and, on the other hand, the choice of aluminum as an isotropic constituting material with relatively high shear rigidity.

To show the merit and reliability of the established approach for the adhesive-bonded multilayer structural elements, a comparison of the first six natural frequencies of a two-layer glass beam bonded by the

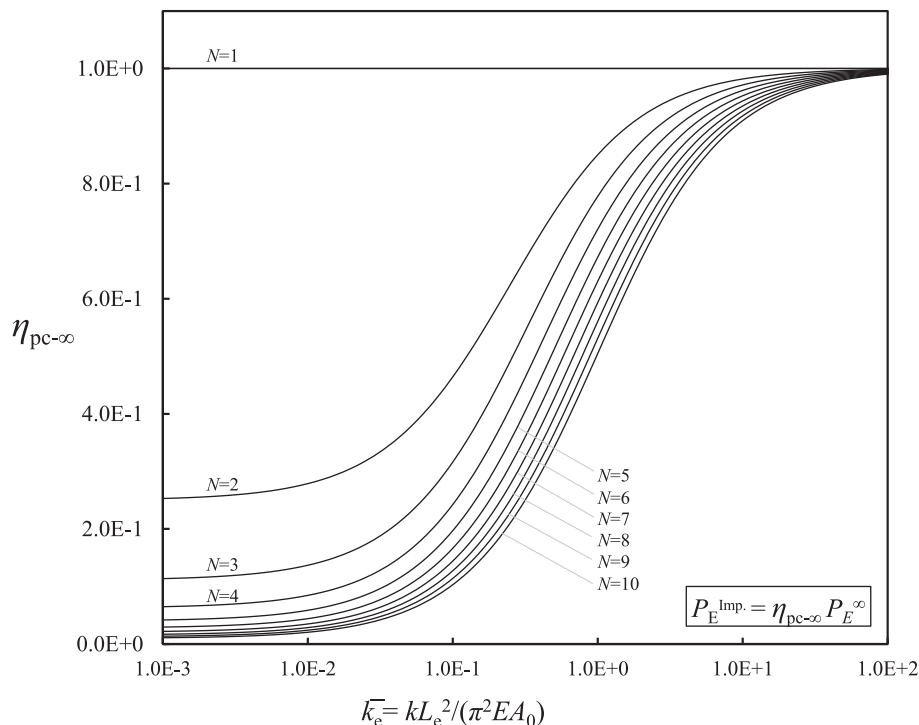


Fig. 5. Variations of the buckling conversion factor, $\eta_{pc-\infty}$, versus the dimensionless interlayer slip modulus, \bar{k}_c , in terms of the columns' effective length, L_e , corresponding to different end conditions. The buckling reduction factor $\eta_{pc-\infty}$ converts the critical buckling load of the ideal classical layered Euler columns, having full-composite-interaction at their layers interfaces, (P_E^∞) to that of the layered columns with imperfect partial-composite interaction at the interlayers ($P_E^{imp.}$). The coefficient $\eta_{pc-\infty} \leq 1$, and the upper-bound unity reflects the perfect case with an integrated cross-section. (N : the number of a column's constituting layers).

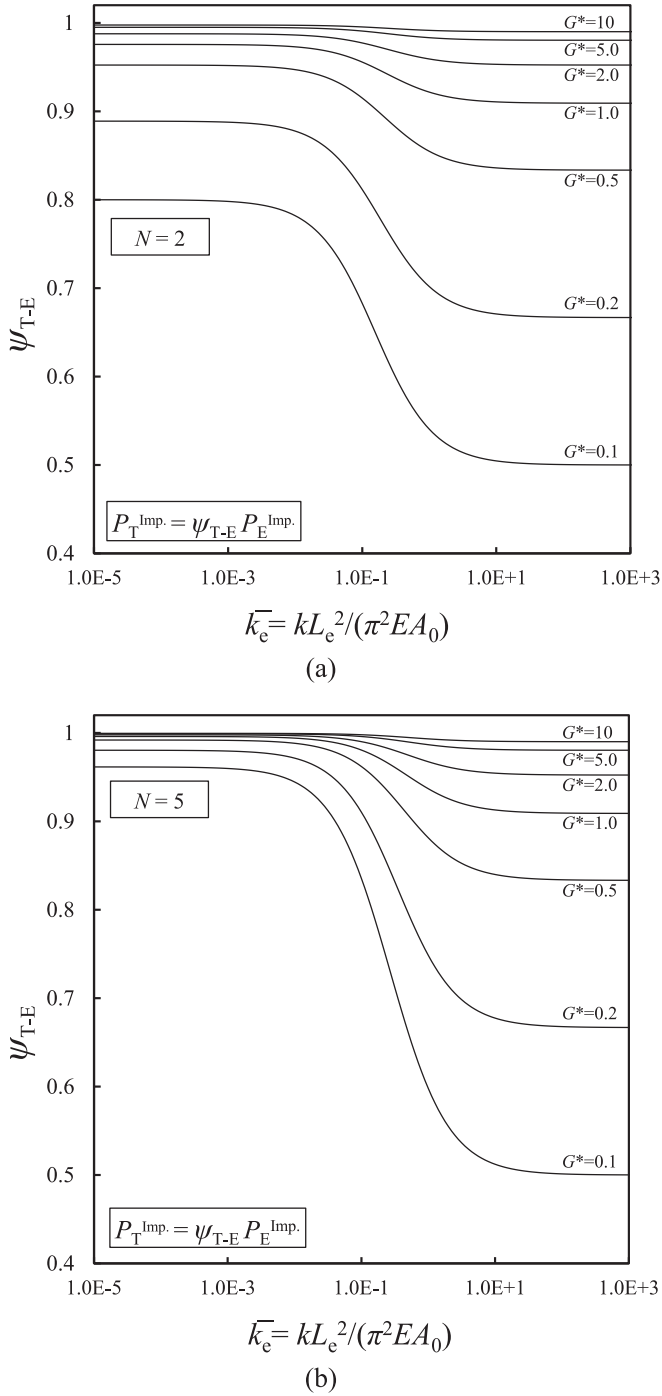


Fig. 6. Variations of the buckling reduction coefficient, ψ_{T-E} , versus the dimensionless interlayer slip modulus, \bar{k}_e (in terms of the columns' effective length, L_e , corresponding to different end conditions), for different levels of shear-effect factor: $G^* = \bar{G}/\bar{h}_e^2 = (GL_e^2)/(\pi^2 E h_{tot}^2) = 0.1, 0.2, 0.5, 1, 2, 5$ and 10 for multilayer columns composed of different number of layers: (a) $N = 2$; (b) $N = 5$. The buckling reduction factor ψ_{T-E} converts the critical buckling loads of the Euler-based partial-composite (EBPC) columns ($P_E^{Imp.}$) to those of Timoshenko/Engesser-based (TEPC) model ($P_T^{Imp.}$); (The reduction coefficient, irrespective of the interlayer interaction level, approaches unity for all cases when the shear-to-Young's modulus ratio of the constituent material tends to a large value; i.e., shear rigidity).

polyvinyl butyral (PVB) elastomeric polymer is provided in Table 5, based on the present approaches and those reported by Sainsbury and Zhang [93] based on the Galerkin element method (GEM) as well as the corresponding results by Koutsawa and Daya [94] using the finite element method (FEM). The geometrical and material property parameters of the two-layer beam are: $E_g = 70.37$ GPa, $G_{PVB} = 0.7037$ MPa, $\rho_g = 2770$ Kg/m³, $\rho_{PVB} = 970$ Kg/m³, $h_g = 1.52$ mm, $L = 177.8$ mm and $b = 12.7$ mm. It is noticeable that the subscripts 'g' and 'PVB' indicate the mentioned property parameter for each glass layer and the PVB bonding layer, respectively.

Here, we calculate the imperfect partial-composite interlayer modulus k according to Eq. (69) to be used in the present models as: $k = G_{PVB}b/h_{PVB} = 70.37$ MPa.

The comparative results of Table 5 reveal that there is a very good agreement between the predicted natural frequencies of the adhesive-bonded glass beam and those reported in the literature using FE analyses, confirming the applicability and reliability of the present models and the introduced simple formulae.

To demonstrate the validity and high accuracy of the present approach and the introduced efficient buckling formulae for the buckling of multilayer partial-composite columns, a comparison of Eqs. (31)-(33) with those available in the literature is provided in the following.

Based on the research conducted in [41] and [61] for the structural analyses of two-layer partial-composite Euler-Bernoulli beam-columns, the following buckling formula was reported for pinned end- (simply-supported), clamped-free- or clamped-clamped columns:

$$\frac{P_{cr}}{P_E^0} = \frac{P_E^0 + a^2 EI_0}{P_E^0 + \frac{EI_0}{EI_\infty} a^2 EI_0} : a^2 = \frac{kr^2}{EI_0 \left(1 - \frac{EI_0}{EI_\infty}\right)} \quad (71)$$

where r is in-depth distance between the centroid of the two layers at the column cross-section. In case of two identical constituting layers, the above equation can be rearranged in the form:

$$P_{cr} = \frac{\pi^2 + 8 \frac{kL_e^2}{EA}}{\pi^2 + 2 \frac{kL_e^2}{EA}} \left(\frac{2\pi^2 EI}{L_e^2} \right) \quad (72)$$

which is obviously exactly the same as that given in Table 1 for the two-layer partial-composite Euler columns on the basis of the introduced Eqs. (31)-(33) (EI and EA are the bending and axial stiffness of each individual layer, respectively).

Furthermore, a comparison of the resulting buckling equation from Table 1 for the partial-composite columns composed of three identical layers (i.e., $EI_\infty = 9EI_0$) with that reported in [66] for a three-layer wood element bonded at its interfaces equivalent to a partial slip modulus k as

$$P_{cr,E} = \frac{\pi^2 + 9k \frac{L_e^2}{EA}}{\pi^2 + k \frac{L_e^2}{EA}} \left(\frac{3\pi^2 EI}{L_e^2} \right) \quad (73)$$

reveals that both are identical, confirming the validity and correctness of the present multilayer composite model and the developed buckling solutions. Moreover, for the case of three-layer pinned-pinned column connected with n mechanical connectors per row of its cross-section with the spacing s between each two adjacent rows of the connectors (each connector with shear connection modulus K [N/m]), Rasmussen and Goodman [95] reported the Euler-kinematics-based buckling equation as

$$P_{cr,E} = \frac{\pi^2 + 9n_{row} \frac{K}{s} \frac{L_e^2}{EA}}{\pi^2 + n_{row} \frac{K}{s} \frac{L_e^2}{EA}} \left(\frac{3\pi^2 EI}{L_e^2} \right) \quad (74)$$

Evidently, the slip modulus k [N/m²] defined in the present study is equivalent to $n_{row}K/s$ (see also Eq. (70) and Fig. 3). Therefore, Eq. (74) is exactly identical to that deduced from Table 1, if we set the effective buckling length $L_e = L$ corresponding to a pinned-pinned or simply-

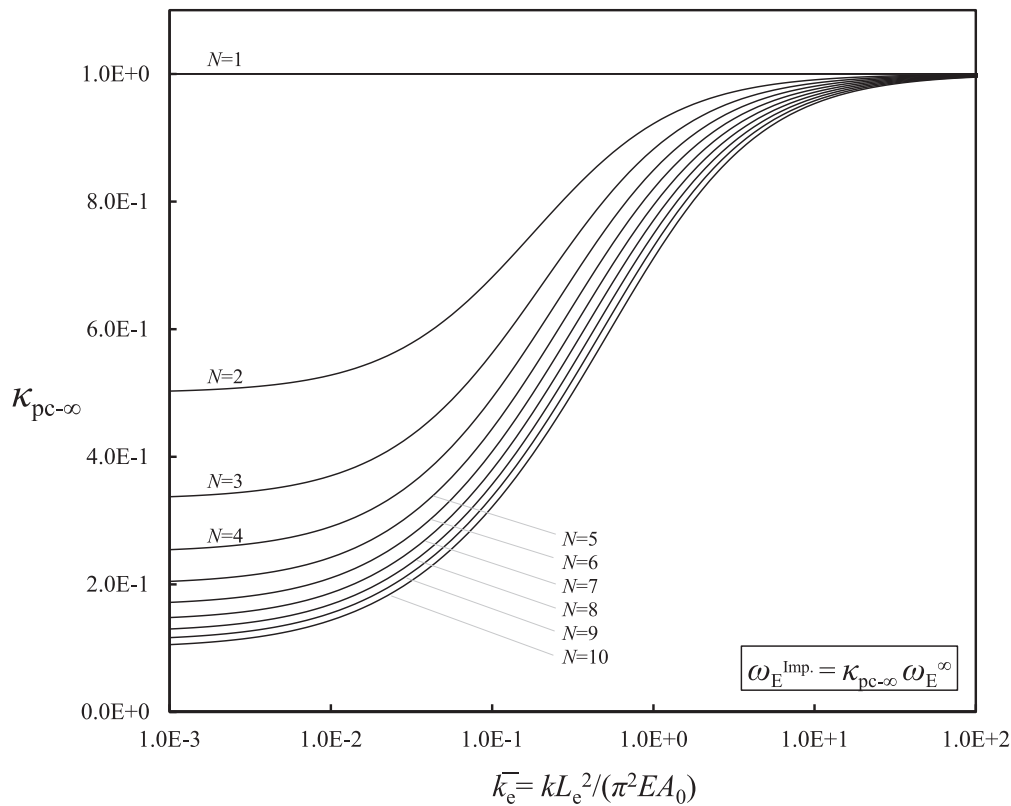


Fig. 7. Variations of the frequency conversion factor, $\kappa_{pc-\infty}$ versus the dimensionless interlayer slip modulus, \bar{k}_e , in terms of the beam element's effective length, L_e , corresponding to different end conditions. The frequency factor $\kappa_{pc-\infty}$ converts the natural frequencies of the ideal multilayer classical layered Euler-Bernoulli beams, having full-composite-interaction at their layers interfaces, (ω_E^{∞}) to those of the layered beams with imperfect partial-composite interaction at the interlayers ($\omega_E^{imp.}$). The coefficient $\kappa_{pc-\infty} \leq 1$, and the upper-bound unity reflects the perfect case with a fully integrated cross-section. (N : the number of a beam's constituting layers).

supported (SS) case.

To demonstrate the validity of the approach for deep multilayer elements composed of a higher number of layers, the Swedish glulam GL30c timber beam product [96] was selected for comparative study using finite element analysis (FEA). The structural element consists of five orthotropic lamellae with low shear rigidity, each of thickness 45 mm (total cross-section height of 225 mm), and the standard width of $b = 140$ mm. The geometrical configuration is illustrated in Fig. 4.

The orthotropic constituting material properties (mean value) [97] are given in Table 6, linked to the property directions shown in Fig. 4. Moreover, the density (mean value) of $\rho_{mean} = 430 \text{ Kg/m}^3$ [97] is considered.

The finite element modelling and analysis of the described glulam beams were carried out using the commercially available software Abaqus/CAE (Dassault Systèmes) for the free vibration analysis. Each of the five lamella layers was modeled by employing the three-dimensional (3-D) solid element type C3D8R, an eight-node brick element with reduced integration and enhanced hourglass control, to achieve accurate results. Each lamella was assigned with an orthotropic section, built up with the elastic property set in Table 6. A thin adhesive layer of average thickness 0.1 mm is modelled between the surfaces of every two adjacent lamellae. A relatively soft-shear isotropic material with flexible values of the shear modulus was assigned, corresponding to different values of the interlayer modulus. The adhesive-lamella coinciding surfaces were constrained via tie-constraint of the elements' nodes. A double-sided bias-pattern fine mesh distribution was implemented for the through-depth element sizing to achieve a denser mesh at the vicinity of the adhesive-lamella interfaces. This was applied to ensure that interaction effects are properly captured, gaining accurate and reliable results.

A comparison of the first five natural frequencies (Hz) of the partial-

composite glulam GL30c beam, extracted from the FEA, is presented in Table 7, alongside those based on both the Euler-Bernoulli-hypothesis-based (EBPC) model and the Timoshenko/Engesser-based partial-composite (TEPC) model. The comparative results are presented for different values of the interlayer interaction modulus, k , ranging from zero interlayer interaction (non-composite) to perfectly-bonded (full-composite) condition. Percentage discrepancy is calculated for any of the EBPC and TEPC cases relative to their corresponding 3-D FEA results.

The results of Table 7 reveal that there is a very good agreement between the 3-D FEA results and those obtained from the proposed TEPC model across all cases, even for the higher modes, regardless of the level of interlayer interaction. It is evident from Table 7, that the maximum percentage discrepancy between the 3-D FEA results and the TEPC model predictions does not exceed 2 % for the analyzed five-layer orthotropic glulam GL30c beam, confirming the validity and accuracy of the introduced TEPC model. However, the percentage discrepancy between the 3-D FEA results and those predicted by the EBPC model significantly increases with an increase in the interlayer interaction level. This error is as high as about 92 % in comparison with the corresponding 3-D FEA result while the error associated with the corresponding value predicted via the TEPC model is less than 1.5 %.

5.3. Results and discussion

Results and discussion are provided here based on the developed analysis approaches for both Euler-Bernoulli- (EBPC) and Timoshenko/Engesser-based partial-composite (TEPC) models and the introduced solutions for the problems of buckling and vibrations of columns and beams having interlayer partial interaction imperfection. The numerical results are presented in a dimensionless format based on the previously-defined effective group of dimensionless parameters.

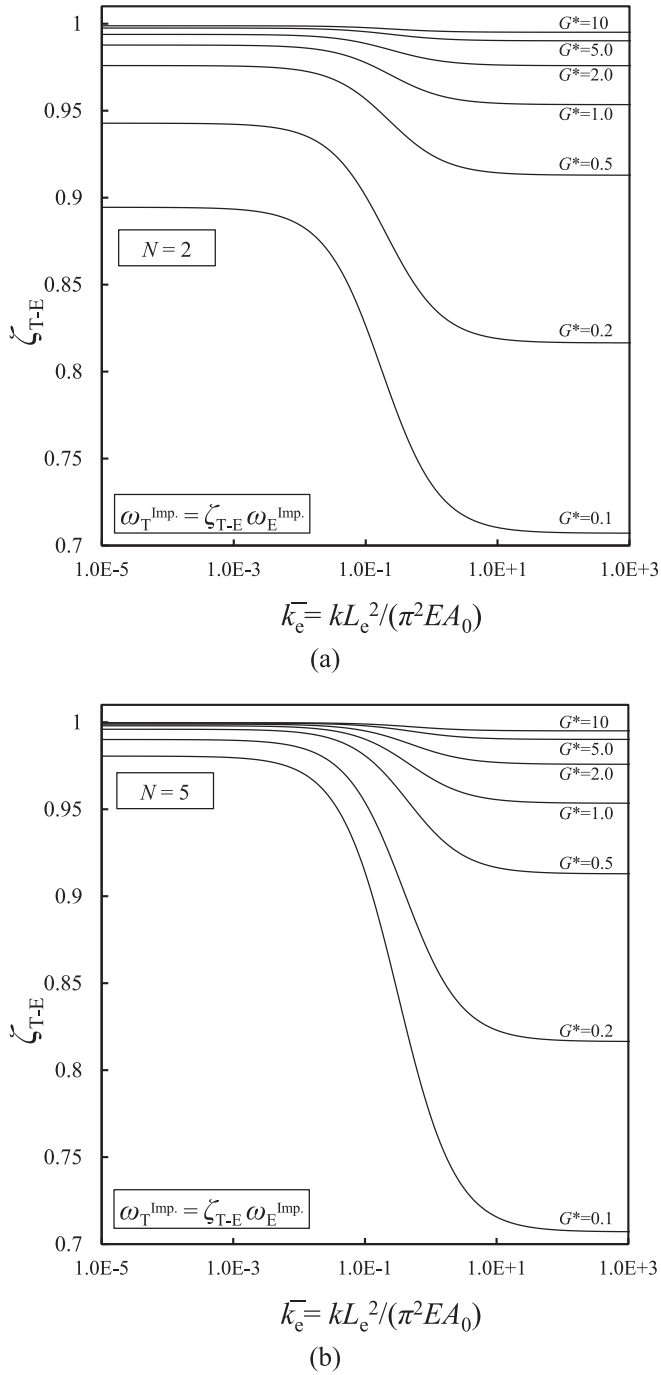


Fig. 8. Variations of the frequency reduction coefficient, ζ_{T-E} , versus the dimensionless interlayer slip modulus, \bar{k}_e (in terms of the beams' effective length, L_e , corresponding to different end conditions), for different levels of shear-effect factor: $G^* = \bar{G}/\bar{h}_e^2 = (GL_e^2)/(\pi^2 E h_{Tot}^2) = 0.1, 0.2, 0.5, 1, 2, 5$ and 10 , for multilayer beams composed of different number of layers: (a) $N = 2$; (b) $N = 5$. The frequency reduction factor ζ_{T-E} converts the fundamental natural frequencies of the Euler-Bernoulli-based partial-composite beams ($\omega_E^{Imp.}$) to those of Timoshenko/Engesser-based partial-composite (TEPC) model ($\omega_T^{Imp.}$); (The reduction coefficient, irrespective of the interlayer interaction level, approaches unity for all cases when the shear-to-Young's modulus ratio of the constituent material tends to a large value; i.e., shear rigidity).

Fig. 5 shows the variation of the buckling conversion factor $\eta_{pc-\infty} = P_E^{Imp.}/P_E^{\infty}$ (the ratio of the critical buckling load of layered partial-composite Euler columns to that of columns with full-composite interaction), versus the dimensionless interlayer slip modulus, \bar{k}_e , in terms of the columns' effective length L_e . The comparative curves are depicted for the imperfect columns composed of different numbers of layers, N , ranging from a single layer to ten layers, while maintaining the total cross-sectional height-to-column length the same. Thus, N represents the number of cross-section divisions, with partial interlayer interaction at their interfaces.

It can be observed that the magnitude of the critical buckling load ratio for partial-composite columns ($\eta_{pc-\infty} = P_E^{Imp.}/P_E^{\infty}$) asymptotically approaches certain lower-bound values and unity when the dimensionless interlayer slip modulus \bar{k}_e approaches zero and infinity, respectively. The lower-bound values reflect special cases in which the frictionless layers lay one another without any interaction (i.e., non-composite), whereas the upper-bound unity represents the unique case of a perfectly-bonded column with fully-integrated cross-section (i.e., $P_{cr} = P_E^{\infty}$). It can be seen from Fig. 5 that there is a quasi-linear relationship between the critical buckling load ratio and the dimensionless interlayer slip modulus in the logarithmic scale for a slip modulus range far from zero and infinity. It can also be deduced from the curves of Fig. 5 that the critical buckling load ratio ($\eta_{pc-\infty} = P_E^{Imp.}/P_E^{\infty}$) of imperfectly-bonded layered columns, having identical cross-section's total height-to-column length ratio, decreases by increasing the number of constituting layers. This highlights the more pronounced influence of interlayer interaction level on the buckling load capacity of the layered columns constituting of a greater number of layers.

To investigate the influence of the disregarded shear deformations in multilayer partial-composite Euler columns on their buckling performance, variations of the Euler-to-Timoshenko/Engesser buckling transition coefficient for imperfect columns ($\psi_{T-E} = P_T^{Imp.}/P_E^{Imp.}$) versus the dimensionless interlayer modulus parameter, \bar{k}_e , are illustrated in Fig. 6a,b, respectively, for columns composed of two and five layers. For each case, different levels of the shear-effect factor $G^* = \bar{G}/\bar{h}_e^2$ are considered, ranging from 0.1 to a relatively large value of 10, representing the layered columns with an extreme shear-softness to relatively shear-rigidity. It should be reminded that the dimensionless parameters group $G^* = \bar{G}/\bar{h}_e^2$ appeared in the final buckling and vibration formulae based on the TEPC model (see Eqs. (56) and (66)), plays an important role in determining the relative shear flexibility effects in the layered beam and column elements. Evidently, all the differences between the buckling and vibration analyses based on the Euler partial-composite model and those according to the TEPC model may be attributed to this parameter. Therefore, we call it the shear-effect parameter: $\pi^2 G^* = \pi^2 \bar{G}/\bar{h}_e^2 = (G/E)(L_e/h_{Tot})^2$. Obviously, the contribution of the reduction of an element's length-to-total depth ratio to its shear deformations is equivalent to a squared reduction of the shear-to-Young's modulus ratio.

It can be seen from Fig. 6a,b that, the Euler-to-Timoshenko/Engesser buckling conversion factor of partial-composite columns, ψ_{T-E} , is always less than unity for all cases, meaning that the Euler partial-composite model unrealistically overpredicts the buckling load capacity of the layered partial-composite columns, similar to the classical Euler columns. However, as can be seen from the curves, the level of error in that model depends on both interlayer imperfect-bonding interaction as well as the number of constituting layers. A comparison of the curves of Fig. 6a,b reveals that the effect of the interlayer modulus parameter on the conversion coefficient is less pronounced for the columns composed of a higher number of layers. Clearly, the conversion factor decreases with a decrease in the shear-effect factor G^* , and it approaches unity when the shear-effect parameter approaches infinity. It can also be deduced from the curves of Fig. 6a,b that the buckling loads over-estimation error in the Euler hypothesis is lower for the imperfect

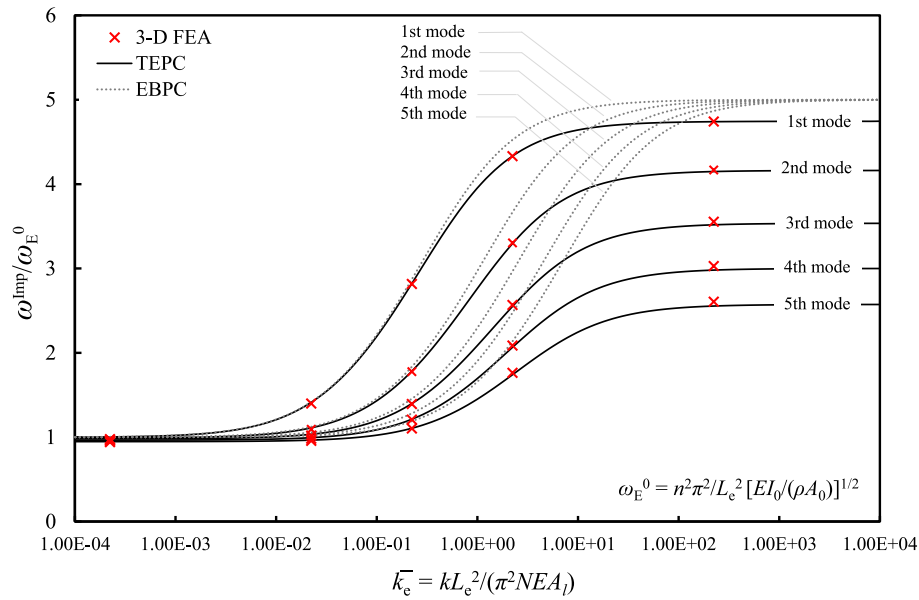


Fig. 9. Variations of the first five natural frequencies of the analyzed five-layer glulam GL30c beam, predicted based on both the EBPC and TEPC models. The 3-D FEA results are shown in the figure.

Table 8

Comparison of the dimensionless natural frequencies (ω_T^{imp}) of imperfect multilayer beams based on the exact nonlinear characteristic equation (65) and those obtained from the introduced simple closed-form vibration formula (66).

			$N = 2$	$N = 5$	$N = 10$	$N = 100$
$\bar{k}_e = 0.1$	$G^* = 0.1$	Exact	0.1615	0.1169	0.0882	0.0305
		Eq. (66)	0.1625	0.1171	0.0882	0.0305
		[% Diff.]	0.6 %	0.2 %	0.0 %	0.0 %
	$G^* = 1.0$	Exact	0.1900	0.1265	0.0921	0.0307
		Eq. (66)	0.1922	0.1269	0.0922	0.0307
		[% Diff.]	1.1 %	0.3 %	0.1 %	0.0 %
$G^* = 10$	Exact	0.1937	0.1276	0.0925	0.0307	
	Eq. (66)	0.1962	0.1280	0.0926	0.0307	
	[% Diff.]	1.2 %	0.3 %	0.1 %	0.0 %	
$\bar{k}_e = 1.0$	$G^* = 0.1$	Exact	0.1939	0.1817	0.1663	0.0854
		Eq. (66)	0.1956	0.1830	0.1672	0.0854
		[% Diff.]	0.8 %	0.7 %	0.5 %	0.0 %
	$G^* = 1.0$	Exact	0.2490	0.2253	0.1981	0.0890
		Eq. (66)	0.2555	0.2291	0.2001	0.0890
		[% Diff.]	2.6 %	1.6 %	1.0 %	0.0 %
$G^* = 10$	Exact	0.2575	0.2315	0.2023	0.0893	
	Eq. (66)	0.2650	0.2358	0.2045	0.0894	
	[% Diff.]	2.9 %	1.8 %	1.0 %	0.1 %	
$\bar{k}_e = 10$	$G^* = 0.1$	Exact	0.2010	0.1996	0.1973	0.1661
		Eq. (66)	0.2031	0.2016	0.1992	0.1669
		[% Diff.]	1.0 %	1.0 %	0.9 %	0.4 %
	$G^* = 1.0$	Exact	0.2642	0.2610	0.2561	0.1978
		Eq. (66)	0.2729	0.2692	0.2635	0.1997
		[% Diff.]	3.2 %	3.1 %	2.8 %	0.9 %
$G^* = 10$	Exact	0.2747	0.2709	0.2651	0.2020	
	Eq. (66)	0.2846	0.2804	0.2740	0.2041	
	[% Diff.]	3.6 %	3.5 %	3.3 %	1.0 %	

columns when compared with the ideal columns. In other words, the highest error in load capacity of multilayer columns based on the Euler partial-composite model is for the perfectly-bonded cases, whereas the lowest error is for the columns with zero layers-interaction (i.e., non-composite).

In Fig. 7, variations of the ratio of the fundamental natural frequency of layered partial-composite beams (ω_E^{imp})-to-that of beams with ideal full-composite interaction (ω_E^∞) are depicted versus the dimensionless interlayer modulus parameter \bar{k}_e in terms of the effective length, according to the EBPC model. Similar to the previous buckling results, the

curves are represented for the beams with identical total cross-sectional height-to-beam ratio, however, with different numbers of constituting layers, to study their influence on the structural behavior of the multilayer partial-composite elements. It can be seen from Fig. 7 that, regardless of the number of constituting layers, the fundamental frequency of the layered partial-composite beams, ω_E^{imp} , approaches to the upper-bound fundamental frequency of the ideal perfectly-bonded beam (ω_E^∞) when the interlayer modulus parameter approaches infinity. It can also be seen that the ratio $\kappa_{pc-\infty} = \omega_E^{imp} / \omega_E^\infty$ tends to certain lower-bound values and unity, respectively, when the interlayer interaction

modulus approaches zero and infinity. In other words, the frequencies of each case approach the lower-bound of a comparable layered element in which there is no bonding interaction between the layers, and the upper-bound of a perfectly-bonded beam having fully-integrated cross-section. It can also be observed from Fig. 7 that, for a practical range of the interlayer interaction parameter far from zero and infinity, there is a quasi-linear correlation between the frequency conversion coefficient, $\kappa_{pc-\infty}$, and the interlayer modulus, \bar{k}_e , in logarithmic scale.

Variations of the reduction factor $\zeta_{T-E} = \omega_T^{\text{Imp}} / \omega_E^{\text{Imp}}$, which converts the natural modal frequencies of the Euler-Bernoulli-based partial-composite beams to those based on the TEPC model, are exhibited in Fig. 8a,b. This provides a better understanding and insight into the level of error associated with using the EBPC model for the frequency analysis of multilayer imperfect beams.

The graphs are provided for various levels of the shear-effect factor G^* , and to investigate the effect of the number of constituting layers on the mentioned error level, the curves are depicted for the elements composed of two and five layers, respectively in Fig. 8a and 8b.

It can be seen from these figures that the highest reduction to the frequencies of the beams based on the EBPC, to be converted to those of the TEPC model, can be attributed to the elements with maximum interlayer interaction (i.e., perfectly-bonded elements) whereas the reduction coefficient is nearly close to unity when there is no bonding and interaction between the layers. However, for all cases, the reduction factor tends to its maximum value (i.e., unity) by increasing the number of constituting layers. It can also be deduced from the figures that a decrease in the shear-effect factor G^* obviously results in decreasing the reduction factor due to the more dominant contribution of the shear softness on the natural frequencies.

To investigate the effect of the previously discussed parameters on the higher vibration modes, variations of the first five natural frequencies of the analyzed five-layer glulam GL30c beams, predicted based on both the EBPC and TEPC models, versus the dimensionless interlayer interaction parameter \bar{k}_e are depicted in Fig. 9. The 3-D FEA results are also included in the figure, to demonstrate the generality of the proposed dimensionless parameters. It can be seen that conclusions drawn for the fundamental natural frequency, predicted by the EBPC and TEPC models, remain valid and true for the higher modes' natural frequencies. It can be deduced from Fig. 9 that the results of the three mentioned sources are in very good agreement for the lower values of dimensionless interlayer interaction parameter, for all the first five vibration modes. However, the predicted results based on EBPC gradually deviate from those of the other methods when the interlayer interaction parameter increases. This holds true, as the effect of shear deformations becomes more dominant when the interlayer interaction increases, and the EBPC model cannot capture the effects of shear deformations.

It can also be observed from Fig. 9 that, unlike the developed TEPC model, the EBPC model cannot inherently capture the effect of the higher vibration modes on the dimensionless frequency parameter $(\omega_E^{\text{Imp}} / \omega_E^0)$. Consequently, the highest error in the natural frequencies predicted by the EBPC is observed to be for the highest modes of a beam with full-composite interaction.

As mentioned in Sections 3.4 and 4.4, the closed-form formulae introduced for the natural frequencies of the multilayer partial-composite beams rely on the key assumption that the effect of constituting layers' axial mass inertia on their vibration behavior is negligible. To demonstrate the validity and high accuracy of the resulted frequencies, a comparison of the results based on Eq. (66) and those extracted from the nonlinear characteristic Eq. (65) is presented in Table 8 for different values of the shear-effect factor, the dimensionless interlayer modulus parameter, as well as different numbers of constituting layers.

It can be seen from Table 8 that the maximum discrepancy between the frequencies predicted from the two mentioned sources is less than

3.7 % for all cases. The small percentage difference between the results of both sources confirms the validity of the introduced simple closed-form vibration formulae.

6. Conclusions

In the present study, an Euler-Bernoulli- (EBPC) and a Timoshenko/Engesser-hypothesis-based partial-composite (TEPC) model were employed, and the stability and vibration problems of columns/beams composed of any number of constituting identical layers, incorporating the effect of interfacial-bonding imperfection in the form of partial-composite interaction, were formulated. The presented novel solutions addressed a known challenging problem in the literature regarding the limitation in the total number of constituting layers of a partially-composite structural element. However, the applicability of the introduced models and the exact analytical solutions is limited to identical constituent layers. A simple efficient conversion coefficient was introduced for the first time in terms of some effective dimensionless parameter groups, converting the well-known classical Euler buckling formulae for the critical loads to that of multilayer partial-composite columns on the basis of exact analytical solutions. Similarly, a coefficient was introduced, enhancing the classical vibration formula of Euler-Bernoulli beams to that for beams composed of N partially-interacting layers. It was shown that the developed general coefficients in terms of the "effective length" can capture different classical end conditions. In continuation of the study, a novel Timoshenko/Engesser-hypothesis-based partial-composite model, as well as exact analytical solutions, were established to treat the governing differential equations and boundary conditions of flexible multilayer shear deformable beams/columns, incorporating the effect of interlayer partial interaction imperfection. Consequently, simple and efficient reduction buckling- and vibration coefficients were introduced for the first time, turning the mentioned Euler-based partial-composite multilayer buckling and vibration formulae into those based on Timoshenko/Engesser partial-composite (TEPC) model. It was shown that the highest reduction to the buckling capacity and frequencies of columns/beams based on the EBPC model, to be converted to those of the TEPC model, occurs for the elements with maximum interlayer interaction, whereas the reduction coefficient is nearly close to unity when there is no bonding and interaction between the layers. It was also concluded that the effect of the interlayer interaction level on the Euler-to-Timoshenko/Engesser conversion coefficients is less pronounced for the elements composed of a higher number of layers.

CRediT authorship contribution statement

Seyed Rasoul Atashipour: Writing – review & editing, Writing – original draft, Visualization, Validation, Software, Resources, Project administration, Methodology, Investigation, Funding acquisition, Formal analysis, Data curation, Conceptualization. **Noël Challamel:** Writing – review & editing, Validation, Project administration, Methodology, Investigation, Funding acquisition, Formal analysis, Data curation, Conceptualization. **Ulf Arne Girhammar:** Writing – review & editing, Project administration, Methodology, Investigation, Funding acquisition, Conceptualization. **Peter D. Folkow:** Writing – review & editing, Project administration, Methodology, Investigation, Funding acquisition, Conceptualization.

Declaration of competing interest

The authors declare that they have no known competing financial interests or personal relationships that could have appeared to influence the work reported in this paper.

Appendix A

Details on the solution for the set of linear second-order difference equations (12b) are presented here. A change-of-variable for the coefficients of the axial displacement components U_i in Eq. (12b) is used as

$$U_i = c\lambda^i, \quad i \in \{1, 2, \dots, N\} \quad (\text{A-1})$$

Substituting Eq. (A-1) into the set of difference Eq. (12b), it can be expressed in the form:

$$\lambda^2 - [2 + 1/(N\bar{k})]\lambda + 1 = 0 \quad (\text{A-2})$$

which obviously gives the following two roots:

$$\lambda_{1,2} = 1 + 1/(2N\bar{k}) \pm \sqrt{1/(2N\bar{k})[1 + 1/(2N\bar{k})]} \quad (\text{A-3})$$

Defining the repeating term $[1 + 1/(2N\bar{k})]$ in Eq. (A-3) as

$$\cosh\theta = 1 + 1/(2N\bar{k}) \quad (\text{A-4})$$

the parameter λ is simplified as

$$\lambda_{1,2} = \cosh\theta \pm \sinh\theta \quad (\text{A-5})$$

Substituting Eq. (A-5) into Eq. (A-1) yields

$$U_i = c_1 e^{i\theta} + c_2 \lambda^{-i\theta} \quad (\text{A-6})$$

or equivalently:

$$U_i = A \cosh i\theta + B \sinh i\theta, \quad i \in \{1, 2, \dots, N\} \quad (\text{A-7})$$

Appendix B

Proof of the general form of the buckling formula presented by Eq. (32) is given here. We consider the definition of the hyperbolic function:

$$\sinh N\theta_e = \frac{e^{N\theta_e} - e^{-N\theta_e}}{2} = \frac{\chi^{2N} - 1}{2\chi^N} \quad (\text{B-1})$$

in which $\chi = e^{\theta_e}$; and for $N = 1$:

$$\sinh\theta_e = \frac{\chi^2 - 1}{2\chi} \quad (\text{B-2})$$

Solving Eq. (B-2) with respect to χ results in

$$\chi = \sinh\theta_e + \sqrt{\sinh^2\theta_e + 1} \equiv \cosh\theta_e + \sqrt{\cosh^2\theta_e - 1} \quad (\text{B-3})$$

Replacing the definition of θ_e from the last of Eq. (25) into the above equation yields

$$\chi = \frac{1}{2N\bar{k}_e} \left(1 + 2N\bar{k}_e + \sqrt{1 + 4N\bar{k}_e} \right) \quad (\text{B-4})$$

Upon substitution of Eq. (B-4) into Eq. (B-1), one can obtain

$$\sinh N\theta_e = \frac{(1 + 2N\bar{k}_e + \sqrt{1 + 4N\bar{k}_e})^{2N} - (2N\bar{k}_e)^{2N}}{2^{N+1} N^N \bar{k}_e^N (1 + 2N\bar{k}_e + \sqrt{1 + 4N\bar{k}_e})^N} \quad (\text{B-5})$$

In a similar procedure, one can obtain the following relation for the function: $\cosh N\theta_e$ in terms of the dimensionless interlayer slip modulus \bar{k}_e , as

$$\cosh N\theta_e = \frac{(1 + 2N\bar{k}_e + \sqrt{1 + 4N\bar{k}_e})^{2N} + (2N\bar{k}_e)^{2N}}{2^{N+1} N^N \bar{k}_e^N (1 + 2N\bar{k}_e + \sqrt{1 + 4N\bar{k}_e})^N} \quad (\text{B-6})$$

Substituting Eqs. (B-5) and (B-6) into the buckling Eq. (25), (noting that $\tanh\theta_e/2 \equiv (\cosh N\theta_e - 1)/\sinh N\theta_e$), it can be presented in the following explicit form:

$$\frac{P}{P_E^0} = 1 + 12\bar{k}_e \left(N - \sqrt{1 + 4N\bar{k}_e} \frac{(1 + 2N\bar{k}_e + \sqrt{1 + 4N\bar{k}_e})^N - (2N\bar{k}_e)^N}{(1 + 2N\bar{k}_e + \sqrt{1 + 4N\bar{k}_e})^N + (2N\bar{k}_e)^N} \right) \quad (\text{B-7})$$

Appendix C

It can be shown that the solution for the natural frequencies of partial-composite beams in section 3.4 can be generalized approximately for different classical end cases via the concept of the “effective eigenmode length” (see [44]) as follows:

$$\bar{\omega}_{n,e} = \frac{n\bar{h}_e}{2\sqrt{3}N} \sqrt{n^2 + 12\bar{k}_e \left[N - \frac{\tanh(N\theta_{n,e}/2)}{\tanh(\theta_{n,e}/2)} \right]}, \quad (n = 1, 2, \dots) \quad (\text{C-1})$$

where

$$\theta_{n,e} = \cosh^{-1} \left[1 + n^2/(2N\bar{k}_e) \right] \quad (\text{C-2})$$

and the effective dimensionless beam thickness, \bar{h}_e , and interlayer slip modulus, \bar{k}_e , are defined in terms of the effective eigenmode length L_e for different classical end conditions as [44]:

Simply-supported (SS):

$$L_e = L \quad (\text{C-3a})$$

Clamped-free/cantilever (CF):

$$L_e = \begin{cases} 1.675L, & n = 1 \\ 2nL/(2n - 1), & n \geq 2 \end{cases} \quad (\text{C-3b})$$

Clamped-clamped (CC):

$$L_e = 2nL/(2n + 1) \quad (\text{C-3c})$$

Clamped-pinned (CP):

$$L_e = 4nL/(4n + 1) \quad (\text{C-3d})$$

in which n is clearly the vibration mode number.

Data availability

Data will be made available on request.

References

- [1] Gao Y, Wang J, Song X, Ding H, Wang H, Bi Y, et al. Investigation on the compressive mechanical properties of ultra-thick CFRP laminates. *Int J Mech Sci* 2023;241:107966.
- [2] Gong S, Ohl S, Klaseboer E, Khoo B. Interaction of a spark-generated bubble with a two-layered composite beam. *J Fluids Struct* 2018;76:336–48.
- [3] Kharghani N, Soares CG. Experimental, numerical and analytical study of buckling of rectangular composite laminates. *European Journal of Mechanics-A/Solids* 2020;79:103869.
- [4] Lemos DM, Marques FD, Ferreira AJ. A review on bistable composite laminates for aerospace applications. *Compos Struct* 2023;117756.
- [5] Krzyżak A, Mazur M, Gajewski M, Drozd K, Komorek A, Przybyłek P. Sandwich structured composites for aeronautics: methods of manufacturing affecting some mechanical properties. *International Journal of Aerospace Engineering* 2016;2016.
- [6] Mrazova M. Advanced composite materials of the future in aerospace industry. *Incas bulletin* 2013;5:139.
- [7] Kazemi ME, Medeau V, Chen Y, Xu Z, Petrinic N, Greenhalgh E, et al. Ballistic performance of bio-inspired hybrid interleaved composite structures suitable for aerospace applications. *Compos A Appl Sci Manuf* 2024;179:107992.
- [8] Luo H, Zhang X, Lu X, Chen K. Bandgap analysis of partial-interaction composite beams periodically attached vibration absorbers. *Int J Mech Sci* 2024;267:109006.
- [9] Walsh J, Kim H-I, Suhr J. Low velocity impact resistance and energy absorption of environmentally friendly expanded cork core-carbon fiber sandwich composites. *Compos A Appl Sci Manuf* 2017;101:290–6.
- [10] Atashipour S, Al-Emrani M. A realistic model for transverse shear stiffness prediction of composite corrugated-core sandwich elements. *Int J Solids Struct* 2017;129:1–17.
- [11] Atashipour SR, Girhammar UA, Al-Emrani M. Exact Lévy-type solutions for bending of thick laminated orthotropic plates based on 3-D elasticity and shear deformation theories. *Compos Struct* 2017;163:129–51.
- [12] Gurvich M, Clavette P, Kim S, Zafiris G, Phan N, Rahman A. Effect of Geometrical Imperfections on Structural Integrity of Laminated Composite Structures: Experimental Approach and Characterization. *Proceedings of the American Society for Composites, 33rd Technical Conference* 2018.
- [13] Andrianov IV, Bolshakov VI, Danishevskiy VV, Weichert D.. Asymptotic simulation of imperfect bonding in periodic fibre-reinforced composite materials under axial shear. *Int J Mech Sci* 2007;49:1344–54.
- [14] Tafsirojjaman T, Dogar AUR, Liu Y, Manalo A, Thambiratnam DP. Performance and design of steel structures reinforced with FRP composites: A state-of-the-art review. *Eng Fail Anal* 2022;138:106371.
- [15] She G-L, Ding H-X. Nonlinear primary resonance analysis of initially stressed graphene platelet reinforced metal foams doubly curved shells with geometric imperfection. *Acta Mech Sin* 2023;39:522392.
- [16] Li Y-P, She G-L. Nonlinear dynamic response of graphene platelets reinforced cylindrical shells under moving loads considering initial geometric imperfection. *Eng Struct* 2025;323:119241.
- [17] Cetkovic M. Influence of initial geometrical imperfections on thermal stability of laminated composite plates using layerwise finite element. *Compos Struct* 2022; 291:115547.
- [18] Hilburger MW, Starnes Jr JH. Effects of imperfections of the buckling response of composite shells. *Thin-Walled Struct* 2004;42:369–97.
- [19] Messenger T. Buckling of imperfect laminated cylinders under hydrostatic pressure. *Compos Struct* 2001;53:301–7.
- [20] Li Y-W, Elishakoff I, Starnes Jr JH, Bushnell D. Effect of the thickness variation and initial imperfection on buckling of composite cylindrical shells: Asymptotic analysis and numerical results by BOSOR4 and PANDA2. *Int J Solids Struct* 1997; 34:3755–67.
- [21] Zhang S, Zhang L, Wang Y, Tao J, Chen X. Effect of ply level thickness uncertainty on reliability of laminated composite panels. *J Reinf Plast Compos* 2016;35: 1387–400.
- [22] Wagner HN, Hühne C, Janssen M. Buckling of cylindrical shells under axial compression with loading imperfections: An experimental and numerical campaign on low knockdown factors. *Thin-Walled Struct* 2020;151:106764.

- [23] Arbozc J. The effect of imperfect boundary conditions on the collapse behavior of anisotropic shells. *Int J Solids Struct* 2000;37:6891–915.
- [24] Debski H, Teter A. Effect of load eccentricity on the buckling and post-buckling states of short laminated Z-columns. *Compos Struct* 2019;210:134–44.
- [25] Khayal OMES. Literature review on imperfection of composite laminated plates. *Journal of microscopy and ultrastructure* 2017;5:119–22.
- [26] Tho NC, Cong PH, Zenkour AM, Doan DH, Van Minh P. Finite element modeling of the bending and vibration behavior of three-layer composite plates with a crack in the core layer. *Compos Struct* 2023;305:116529.
- [27] Ladevèze P, Lubineau G, Violeau D. A computational damage micromodel of laminated composites. *Int J Fract* 2006;137:139–50.
- [28] Chen W, Cai J, Ye G. Exact solutions of cross-ply laminates with bonding imperfections. *AIAA J* 2003;41:2244–50.
- [29] Chen W, Ying J, Cai J, Ye G. Benchmark solution of laminated beams with bonding imperfections. *AIAA J* 2004;42:426–9.
- [30] Librescu L, Schmidt R. A general linear theory of laminated composite shells featuring interlaminar bonding imperfections. *Int J Solids Struct* 2001;38:3355–75.
- [31] Ye J, Chen X, Zhai Z, Li B, Zi Y, He Z. Effects of thermal stress and imperfect interfacial bonding on the mechanical behavior of composites subjected to off-axis loading. *Mater Sci Eng A* 2010;527:7530–7.
- [32] Talebitooti R, Daneshjou K, Tarkashvand A. Study of imperfect bonding effects on sound transmission loss through functionally graded laminated sandwich cylindrical shells. *Int J Mech Sci* 2017;133:469–83.
- [33] Diaz AD, Chataigner S, Caron J-F. A layerwise finite element for multilayers with imperfect interfaces. *Compos Struct* 2011;93:3262–71.
- [34] Garg N, Chakladar ND, Prusty BG, Song C, Phillips AW. Modelling of laminated composite plates with weakly bonded interfaces using scaled boundary finite element method. *Int J Mech Sci* 2020;170:105349.
- [35] Zhang D-D, Ren J-J, Gu J, Li L-J, Zhang J-Y, Xiong W-H, et al. Nondestructive testing of bonding defects in multilayered ceramic matrix composites using THz time domain spectroscopy and imaging. *Compos Struct* 2020;251:112624.
- [36] Kapuria S, Dhanesh N. Free edge stresses in composite laminates with imperfect interfaces under extension, bending and twisting loading. *Int J Mech Sci* 2016;113:148–61.
- [37] Li D, Liu Y. Three-dimensional semi-analytical model for the static response and sensitivity analysis of the composite stiffened laminated plate with interfacial imperfections. *Compos Struct* 2012;94:1943–58.
- [38] Feng X, Fan X, Li Y, Zhang H, Zhang L, Gao Y. Static response and free vibration analysis for cubic quasicrystal laminates with imperfect interfaces. *European Journal of Mechanics-A/Solids* 2021;90:104365.
- [39] Yan W, Wang J, Chen W. Cylindrical bending responses of angle-ply piezoelectric laminates with viscoelastic interfaces. *App Math Model* 2014;38:6018–30.
- [40] Wang Z-X, Qiao P, Xu J. Vibration analysis of laminated composite plates with damage using the perturbation method. *Compos B Eng* 2015;72:160–74.
- [41] Girhammar UA, Pan DH. Exact static analysis of partially composite beams and beam-columns. *Int J Mech Sci* 2007;49:239–55.
- [42] Girhammar UA. Composite beam-columns with interlayer slip—approximate analysis. *Int J Mech Sci* 2008;50:1636–49.
- [43] Girhammar UA. A simplified analysis method for composite beams with interlayer slip. *Int J Mech Sci* 2009;51:515–30.
- [44] Girhammar UA, Pan DH, Gustafsson A. Exact dynamic analysis of composite beams with partial interaction. *Int J Mech Sci* 2009;51:565–82.
- [45] Stüssi F. *Zusammengesetzte vollwandträger* IABSE Publications 1947;8:249–69.
- [46] Rzhantsyn AR. *Analysis of built-up rods of structural elements* (in Russian). Moscow 1948.
- [47] Granholm H. *On composite beams and columns with special regard to nailed timber structures* (in Swedish). Gothenburg: Chalmers University of Technology; 1949.
- [48] Newmark NM. Test and analysis of composite beam with incomplete interaction. *Proc of the society for experimental stress analysis* 1951;9:75–92.
- [49] Pleshkov PF. *Theoretical studies of composite wood structures* (in Russian). Moscow 1952.
- [50] Faella C, Martinelli E, Nigro E. Steel and concrete composite beams with flexible shear connection: “exact” analytical expression of the stiffness matrix and applications. *Comput Struct* 2002;80:1001–9.
- [51] Ranzi G, Bradford M, Uy B. A general method of analysis of composite beams with partial interaction. *Steel Compos Struct* 2003;3:169–84.
- [52] Jurkiewicz B, Buzon S, Sieffert J. Incremental viscoelastic analysis of composite beams with partial interaction. *Comput Struct* 2005;83:1780–91.
- [53] Ranzi G, Bradford M. Analytical solutions for the time-dependent behaviour of composite beams with partial interaction. *Int J Solids Struct* 2006;43:3770–93.
- [54] Xu R, Wu Y. Static, dynamic, and buckling analysis of partial interaction composite members using Timoshenko’s beam theory. *Int J Mech Sci* 2007;49:1139–55.
- [55] Schnabl S, Planinc I. The effect of transverse shear deformation on the buckling of two-layer composite columns with interlayer slip. *Int J Non Linear Mech* 2011;46:543–53.
- [56] Santos HA, Silberschmidt VV. Hybrid equilibrium finite element formulation for composite beams with partial interaction. *Compos Struct* 2014;108:646–56.
- [57] Ecsedi I, Baksa A. Analytical solution for layered composite beams with partial shear interaction based on Timoshenko beam theory. *Eng Struct* 2016;115:107–17.
- [58] Challamel N. On lateral-torsional vibrations of elastic composite beams with interlayer slip. *J Sound Vib* 2009;325:1012–22.
- [59] Challamel N, Bernard F, Casandjian C. Out-of-plane behaviour of partially composite or sandwich beams by exact and finite element methods. *Thin-Walled Struct* 2010;48:561–80.
- [60] He G, Yang X. Dynamic analysis of two-layer composite beams with partial interaction using a higher order beam theory. *Int J Mech Sci* 2015;90:102–12.
- [61] Challamel N, Girhammar UA. Variationally-based theories for buckling of partial composite beam-columns including shear and axial effects. *Eng Struct* 2011;33:2297–319.
- [62] Challamel N, Girhammar UA. Lateral-torsional buckling of vertically layered composite beams with interlayer slip under uniform moment. *Eng Struct* 2012;34:505–13.
- [63] Challamel N. On geometrically exact post-buckling of composite columns with interlayer slip—the partially composite elastica. *Int J Non Linear Mech* 2012;47:7–17.
- [64] Le Grogneq P, Nguyen Q-H, Hjjaj M. Exact buckling solution for two-layer Timoshenko beams with interlayer slip. *Int J Solids Struct* 2012;49:143–50.
- [65] Komijani M, Reddy J, Eslami M, Bateni M. An analytical approach for thermal stability analysis of two-layer Timoshenko beams. *Int J Struct Stab Dyn* 2013;13:1350036.
- [66] Atashipour SR, Girhammar UA, Challamel N. Stability analysis of three-layer shear deformable partial composite columns. *Int J Solids Struct* 2017;106:213–28.
- [67] Atashipour SR, Challamel N, Girhammar UA. On buckling of layered composite heavy columns—Effect of interlayer bonding imperfection. *Int J Solids Struct* 2023;260:112030.
- [68] Nguyen H-N, Nguyen T-Y, Tran KV, Tran TT, Nguyen T-T, Phan V-D, et al. A finite element model for dynamic analysis of triple-layer composite plates with layers connected by shear connectors subjected to moving load. *Materials* 2019;12:598.
- [69] Sun Q, Liu X, Zhang N. An accurate solution method for the dynamic characteristics of three-layered partial-interaction composite beams. *Structures: Elsevier*; 2023.
- [70] Lin J-P, Liu X, Wang Y, Xu R, Wang G. Static and dynamic analysis of three-layered partial-interaction composite structures. *Eng Struct* 2022;252:113581.
- [71] Atashipour SR, Girhammar UA, Challamel N. A weak shear web model for deflection analysis of deep composite box-type beams. *Eng Struct* 2018;155:36–49.
- [72] Heinisuo M. An exact finite element technique for layered beams. *Comput Struct* 1988;30:615–22.
- [73] Krawczyk P, Frey F, Zieliński A. Large deflections of laminated beams with interlayer slips: Part 1: model development. *Eng Comput* 2007;24:17–32.
- [74] Krawczyk P, Rebora B. Large deflections of laminated beams with interlayer slips: Part 2: finite element development. *Eng Comput* 2007;24:33–51.
- [75] Ranzi G. Locking problems in the partial interaction analysis of multi-layered composite beams. *Eng Struct* 2008;30:2900–11.
- [76] Sousa Jr JBM, da Silva AR. Analytical and numerical analysis of multilayered beams with interlayer slip. *Eng Struct* 2010;32:1671–80.
- [77] Keo P, Nguyen Q-H, Somja H, Hjjaj M. Derivation of the exact stiffness matrix of shear-deformable multi-layered beam element in partial interaction. *Finite Elem Anal Des* 2016;112:40–9.
- [78] Adam C, Ladurner D, Furtmüller T. Moderately large vibrations of flexibly bonded layered beams with initial imperfections. *Compos Struct* 2022;299:116013.
- [79] Håggbom I. On buckling of a strut composed of several longitudinal elements (in Swedish). *Teknisk Tidskrift (Sweden)* 1941;71:365–8.
- [80] Ylinen A. On buckling of a strut composed of a number of longitudinal elements, specifically with application to the Sandö Bridge. *Teknisk Tidskrift (Sweden)* 1942;72:391.
- [81] Bolotin VV. On the theory of layered plates. *Izv Akad Nauk SSSR Otd Tekh Nauk, Mekh Mashinostr* 1963;3:65–72.
- [82] Bolotin VV, Novichkov YN. *Mechanics of Multilayered Structures*. Moscow: Mashinostroenie; 1980. in Russian.
- [83] Peng S, Zhu Z, Wei Y. An analytic solution for bending of multilayered structures with interlayer-slip. *Int J Mech Sci* 2024;282:109642.
- [84] Shen X, Wei Y, Liu Y. Unlocking slip-mediated bending in multilayers: Efficient modeling and solutions with high precision and simplicity. *Int J Solids Struct* 2024;302:112971.
- [85] Grundberg S, Girhammar UA, Hassan OA. Vibration of axially loaded and partially interacting composite beams. *Int J Struct Stab Dyn* 2014;14:1350047.
- [86] Belinha J, Araújo A, Ferreira A, Dinis L, Jorge RN. The analysis of laminated plates using distinct advanced discretization meshless techniques. *Compos Struct* 2016;143:165–79.
- [87] Bedford A. *Hamilton’s principle in continuum mechanics*. Austin, TX, USA: Springer; 2021.
- [88] Goldberg S. *Introduction to difference equations with illustrative examples from economics, psychology and sociology*. New York: Dover Publications; 1958.
- [89] Girhammar UA, Gopu VK. Composite beam-columns with interlayer slip—exact analysis. *J Struct Eng* 1993;119:1265–82.

- [90] McCutcheon WJ. Method for predicting the stiffness of wood-joint floor systems with partial composite action: Department of Agriculture. Forest Products Laboratory: Forest Service; 1977.
- [91] Design of timber structures. 2:2016 ed: Swedish Forest Industries Federation, 2016.
- [92] Henghold WM. Layered beam vibrations including slip. Colorado State University; 1972.
- [93] Sainsbury M, Zhang Q. The Galerkin element method applied to the vibration of damped sandwich beams. *Comput Struct* 1999;71:239–56.
- [94] Koutsawa Y, Daya EM. Static and free vibration analysis of laminated glass beam on viscoelastic supports. *Int J Solids Struct* 2007;44:8735–50.
- [95] Rassam HY, Goodman J. Buckling behavior of layered wood columns. *Wood Science* 1970;2:238–46.
- [96] Fröbel J. The Glulam Handbook, Volume 1: Facts about glulam. 1:2024 ed. Stockholm, Sweden: Swedish Wood, 2024.
- [97] Godonou P. Design of timber structures, Volume 2: Rules and formulas according to Eurocode 5. 3:2022 ed. Stockholm, Sweden: Swedish Wood, 2022.